Functional Dysregulation of CDC42 Causes Diverse Developmental Phenotypes

Simone Martinelli,[1] Oliver H.F. Krumbach,[2,30] Francesca Pantaleoni,[3,30] Simona Coppola,[4,30] Ehsan Amin,[2,31] Luca Pannone,[3] Kazem Nouri,[2,32] Luciapia Farina,[4] Radovan Dvorsky,[2] Francesca Lepri,[3] Marcel Buchholzer,[2] Raphael Konopatzki,[2] Laurence Walsh,[5] Katelyn Payne,[5] Mary Ella Pierpont,[6,7] Samantha Schrier Vergano,[8] Katherine G. Langley,[9] Douglas Larsen,[10] Kelly D. Farwell,[11] Sha Tang,[11] Cameron Mroske,[11] Ivan Gallotta,[12] Elia Di Schiavi,[12] Matteo della Monica,[13] Licia Lugli,[14] Cesare Rossi,[15] Marco Seri,[16] Guido Cocchi,[16] Lindsay Henderson,[9] Berivan Baskin,[9] Mariëlle Alders,[17] Roberto Mendoza-Londono,[18,19,20] Lucie Dupuis,[18] Deborah A. Nickerson,[21] Jessica X. Chong,[22] The University of Washington Center for Mendelian Genomics, Naomi Meeks,[23] Kathleen Brown,[23] Tahnee Causey,[24] Megan T. Cho,[9] Stephanie Demuth,[25] Maria Cristina Digilio,[3] Bruce D. Gelb,[26] Michael J. Bamshad,[21,22] Martin Zenker,[27] Mohammad Reza Ahmadian,[2,33] Raoul C. Hennekam,[28,33] Marco Tartaglia,[3,33,*] and Ghayda M. Mirzaa[22,29,33,*]

Exome sequencing has markedly enhanced the discovery of genes implicated in Mendelian disorders, particularly for individuals in whom a known clinical entity could not be assigned. This has led to the recognition that phenotypic heterogeneity resulting from allelic mutations occurs more commonly than previously appreciated. Here, we report that missense variants in *CDC42*, a gene encoding a small GTPase functioning as an intracellular signaling node, underlie a clinically heterogeneous group of phenotypes characterized by variable growth dysregulation, facial dysmorphism, and neurodevelopmental, immunological, and hematological anomalies, including a phenotype resembling Noonan syndrome, a developmental disorder caused by dysregulated RAS signaling. *In silico*, *in vitro*, and *in vivo* analyses demonstrate that mutations variably perturb CDC42 function by altering the switch between the active and inactive states of the GTPase and/or affecting CDC42 interaction with effectors, and differentially disturb cellular and developmental processes. These findings reveal the remarkably variable impact that dominantly acting *CDC42* mutations have on cell function and development, creating challenges in syndrome definition, and exemplify the importance of functional profiling for syndrome recognition and delineation.

The rate of identification of genes implicated in human disorders has dramatically increased with the use of second-generation sequencing technologies. In particular, exome sequencing has emerged as a feasible and efficient strategy to uncover the molecular basis of Mendelian disorders, particularly for individuals with a rare clinical presentation or for whom a unifying clinical diagnosis is not discerned.[1] Mutations affecting the same gene but resulting in substantial phenotypic differences is a very well-known phenomenon, but the wide use of exome sequencing has led to the recognition that this event occurs much more commonly than previously appreciated.[2–4] In the last few years, it has been recognized that the variable clinical manifestation of allelic mutations can often result from their differential impact on protein function, although the consequences of specific variants

[1]Department of Oncology and Molecular Medicine, Istituto Superiore di Sanità, Rome 00161, Italy; [2]Institute of Biochemistry and Molecular Biology II, Medical Faculty of the Heinrich-Heine University, Düsseldorf 40225, Germany; [3]Genetics and Rare Diseases Research Division, Ospedale Pediatrico Bambino Gesù, IRCCS, Rome 00146, Italy; [4]National Center for Rare Diseases, Istituto Superiore di Sanità, Rome 00161, Italy; [5]Riley Hospital for Children, Indianapolis, IN 46202, USA; [6]Department of Pediatrics, University of Minnesota, Minneapolis, MN 55454, USA; [7]Children's Hospital of Minnesota, Minneapolis, MN 55454, USA; [8]Division of Medical Genetics and Metabolism, Children's Hospital of The King's Daughters, Norfolk, VA 23507, USA; [9]GeneDX, Gaithersburg, MD 20877, USA; [10]Department of Neurology, Washington University, St. Louis, MO 63130, USA; [11]Ambry Genetics, Department of Clinical Genomics, Aliso Viejo, CA 92656, USA; [12]Institute of Biosciences and Bioresources, National Research Council, 80131 Naples, Italy; [13]Genetica Medica, Azienda Ospedaliera Universitaria Meyer, 50139 Florence, Italy; [14]Struttura Complessa di Neonatologia, Policlinico di Modena, 41124 Modena, Italy; [15]Genetica Medica, Policlinico S.Orsola-Malpighi, 40138 Bologna, Italy; [16]Department of Medical and Surgical Sciences, University of Bologna, 40138 Bologna, Italy; [17]Department of Clinical Genetics, Academic Medical Centre, University of Amsterdam, Amsterdam 1105-AZ, the Netherlands; [18]Division of Clinical and Metabolic Genetics, The Hospital for Sick Children, Toronto, ON M5G 1X8, Canada; [19]Genetics and Genome Biology, The Hospital for Sick Children, Toronto, ON M5G 1X8, Canada; [20]Department of Pediatrics, University of Toronto, Toronto, ON M5G 1X8, Canada; [21]Department of Genome Sciences, University of Washington, Seattle, WA 98195, USA; [22]Department of Pediatrics, University of Washington, Seattle, WA 98195, USA; [23]Children's Hospital Colorado, Aurora, CO 80045, USA; [24]Department of Human and Molecular Genetics, Virginia Commonwealth University, Richmond, VA 23284, USA; [25]Praxis für Humangenetik Erfurt, Erfurt 99084, Germany; [26]Mindich Child Health and Development Institute and Departments of Pediatrics, and Genetics and Genomic Sciences, Icahn School of Medicine at Mount Sinai, New York, NY 10029, USA; [27]Institute of Human Genetics, University Hospital Magdeburg, Magdeburg 39120, Germany; [28]Department of Pediatrics, Academic Medical Center, University of Amsterdam, Amsterdam 1105-AZ, the Netherlands; [29]Center for Integrative Brain Research, Seattle Children's Research Institute, Seattle, WA 98101, USA
[30]These authors contributed equally to this work
[31]Present address: Institute of Neural and Sensory Physiology, Medical Faculty of the Heinrich-Heine University, Düsseldorf, Germany
[32]Present address: Department of Pathology and Molecular Medicine, Richardson Laboratory, Queen's University, Kingston, ON K7L 3N6, Canada
[33]These authors contributed equally to this work
*Correspondence: marco.tartaglia@opbg.net (M.T.), gmirzaa@u.washington.edu (G.M.M.)
https://doi.org/10.1016/j.ajhg.2017.12.015.

can be difficult to predict and may require substantial efforts to be fully understood.[5–7] Here, we report that missense mutations in *cell division cycle 42* (*CDC42* [MIM: 116952]), a gene encoding a member of the RAS superfamily of low-molecular-weight GTP/GDP-binding proteins functioning as a major node in intracellular signaling, underlie a clinically heterogeneous group of developmental phenotypes. Our *in silico*, *in vitro*, and *in vivo* dissection of the structural and functional impact of disease-causing mutations documents that they variably perturb CDC42 biochemical behavior and differentially affect cellular and developmental processes, highlighting the variable impact of the functional dysregulation of this GTPase in cell physiology and development. Our findings also exemplify the importance of functional profiling for syndrome recognition and delineation.

A total of 15 subjects from 13 unrelated families were included in the study. Clinical data and DNA samples were collected from the participating families (after written informed consent was obtained) and stored and used under research projects approved by the Review Boards of the participating institutions. Investigators studying the affected individuals described here were connected via the MatchMaker Exchange (MME) network of web-based tools[8] GeneMatcher and MyGene2.[9,10] Nine affected individuals (subjects 1 to 5 and 8 to 11), who exhibited a molecularly unexplained and clinically unrecognized multi-systemic disorder, were investigated by whole-exome sequencing (WES) using DNA samples obtained from either leukocytes or saliva specimens, and a child-parent trio-based strategy. Exome capture was carried out using the SureSelect Clinical Research Exome (Agilent) (subjects 1 and 8), SureSelect Human All Exon v.1, v.3, and v.5 (Agilent) (subjects 2, 10, and 5, respectively), Nextera Exome Enrichment Kit (Illumina) (subject 3), SeqCap EZ VCRome 2.0 (Roche) (subject 4), and SeqCap EZ MedExome v2 (Roche) (subjects 9 and 11) target enrichment kits, and sequencing was performed on a HiSeq 2000 platform (Illumina), using paired-end. WES data processing, sequence alignment to GRCh37, and variant filtering and prioritization by allele frequency, predicted functional impact, and inheritance models were performed as previously described.[11–13] Mean coverage of target regions and average reads depth for individual samples are provided in Table S1. Subjects 12 (simplex case subject) and 13 to 15 (affected members of family 30153) (Figure S1) belonged to a cohort of 235 unrelated individuals with clinical features fitting Noonan syndrome (MIM: 163950) or overlapping with this disorder, followed at three participating genetic centers (Rome, Bologna, and Magdeburg),[14,15] who did not harbor mutations in previously identified genes implicated in RASopathies. Based on the hypothesis that mutations in *CDC42* might be linked causally to Noonan syndrome (or a clinically related RASopathy), the entire *CDC42* coding sequence was analyzed by targeted resequencing, using genomic DNA from blood, skin fibroblasts, hair bulbs, and/or epithelial cells from the oral mucosa. Target enrichment was performed using the Nextera Rapid Capture kit (Illumina), and sequencing was carried out on a NextSeq550 (Illumina) with a 2 × 150 bp paired-end read protocol. Alignment and variant calling were performed with the BWA Enrichment BaseSpace App (Illumina), and VCF output files were annotated using Variant Studio v.2.2 (Illumina). Finally, Sanger sequencing was used to screen the *CDC42* coding exons in subjects 6 and 7, who showed clinical features suggestive for the condition associated with *CDC42* group I mutations (see below).

Overall, nine different missense mutations distributed across the entire *CDC42* coding sequence were identified (Table 1). Two amino acid substitutions affected the N-terminal α helix (residues Ile21 and Tyr23), three involved adjacent residues within the switch II motif (Tyr64, Arg66, and Arg68), two mapped to the fourth β strand (Cys81 and Ser83), and the remaining two were located close to the C terminus (Ala159 and Glu171) (Figure 1A). Four variants were recurrent, and all occurred as a *de novo* event in at least one family. Of note, the c.511G>A substitution (p.Glu171Lys) was shared by the four affected subjects with clinical features resembling Noonan syndrome, occurring *de novo* in subject 12, and co-segregating with the phenotype in family 30153 (subjects 13 to 15), consistent with dominant inheritance. None of these variants had been reported in ExAC/gnomAD, and all were predicted to be pathogenic and met the American College of Medical Genetics (ACMG) criteria to be considered disease causing (Table S2).[19] One variant, c.191A>G (p.Tyr64Cys), had previously been reported in two subjects with syndromic thrombocytopenia (MIM: 616737).[20,21]

CDC42 encodes a small GTPase of the RHO family modulating multiple signaling pathways controlling cell polarity and migration, endocytosis, and cell cycle progression, by cycling between an active (GTP-bound) and an inactive (GDP-bound) state.[22,23] It is characterized by five major highly conserved motifs, G1 to G5, which mediate GTP binding and hydrolysis (G4 and G5), phosphate binding (G1 and G3), and effector binding (G2) (Figure 1A).[24,25] Based on clinical heterogeneity (see below) and location of affected residues, we predicted that the mutations would have a variable functional impact. The structural consequences of the identified disease-causing mutations on CDC42 structure and function were assessed by Pymol molecular viewer (see Web Resources), using available PDB structures. This allowed us to inspect CDC42 interactions with ARHGAP1 ($p50^{GAP}$/CDC42GAP; PDB: 1grn), ARHGAP18 (MacGAP; PDB: 5c2j), and ITSN1 (PDB: 1ki1) and WAS (WASP; PDB: 1cee), as representatives for CDC42's GTPase activating proteins (GAPs), guanine nucleotide exchange factors (GEFs), and effectors, respectively, and to classify them structurally and functionally into three different groups. A first group of mutations affected the switch II region (p.Tyr64Cys, p.Arg66Gly, and p.Arg68Gln; group I), which mediates CDC42 binding to effectors and regulators (Figures 1B–1D).[25] Tyr64 and

Table 1. List of the Germline *CDC42* Missense Mutations Identified in This Study

Exon	Nucleotide Change	Amino Acid Change	Domain	Mutation Group	Subjects	Origin	MetaSVM[a]	CADD phred[a]	REVEL[a]	ACMG
1	c.62T>C	p.Ile21Thr	α1	III	1	*de novo*	0.3729	27.1	0.901	pathogenic
1	c.68A>G	p.Tyr23Cys	α1	III	2	*de novo*	0.7752	27.1	0.937	pathogenic
3	c.191A>G	p.Tyr64Cys	switch II	I	3	*de novo*	0.7976	23.4	0.834	pathogenic
3	c.196A>G	p.Arg66Gly	switch II	I	4, 5	*de novo*	0.5326	26.9	0.836	pathogenic
3	c.203G>A	p.Arg68Gln	switch II	I	6, 7	*de novo*	0.6586	26.3	0.827	pathogenic
3	c.242G>T	p.Cys81Phe	β4	II	8	*de novo*	0.6280	30.0	0.840	pathogenic
3	c.247T>C	p.Ser83Pro	β4	II	9, 10	*de novo*	0.8283	27.8	0.853	pathogenic
4	c.476C>T	p.Ala159Val	NBP	II	11	*de novo*	1.0179	34.0	0.916	pathogenic
5	c.511G>A[b]	p.Glu171Lys	CBR	III	12, 13–15	1 *de novo*, 1 familial	0.0158	24.7	0.768	pathogenic

Nucleotide numbering reflects cDNA numbering with 1 corresponding to the A of the ATG translation initiation codon in the *CDC42* reference sequence (GenBank: NM_001791.3). No variants were reported in the public databases ExAC and GnomAD. All variants were predicted to be "deleterious" by Combined Annotation Dependent Depletion (CADD) v.1.3, Database for Nonsynonymous SNPs' Functional Predictions (dbNSFP) Support Vector Machine (SVM) v.3.0, and REVEL algorithms.[16–18] All changes satisfied the necessary criteria to be classified as pathogenic according to the American College of Medical Genetics guidelines.[19] Abbreviations: NBP, nucleotide binding pocket; CBR, CRIB motif binding region.

[a]Scores > 0 (MetaSVM), > 15 (CADDphred) or > 0.5 (REVEL) predict that the sequence change has a significant impact on protein structure and function.

[b]This change affects transcript variant 1 (GenBank: NM_001791.3) and isoform 1 (GenBank: NP_001782.1), while it does not affect transcript variant 2 (GenBank: NM_044472.2) and isoform 2 (GenBank: NP_426359.1). The two isoforms have the same amino acid length but are characterized by a different C terminus.

Arg66 are located on the surface of CDC42 and directly participate in interactions with regulatory proteins and effectors. These changes were predicted to affect these interactions and, as a consequence, the catalytic activity of the GTPase and/or its capability to transduce signaling. Similarly, Arg68 is embedded in the protein interior and stabilizes the conformation of the switch II region via intramolecular interactions with multiple residues (Ala59, Gln61, and Glu100). The Arg-to-Gln change was assumed to strongly destabilize the switch II loop and the interaction with signaling partners. Group II included substitutions involving residues located within (Ala159) or close to (Cys81 and Ser83) the nucleotide-binding pocket (Figures 1B, 1C, and 1E). Ala159 faces the guanine base and replacement by valine was predicted to promote fast GDP/GTP cycling, favoring a GEF-independent active, GTP-bound state of the protein. A similar hyperactive behavior has been reported in RAS proteins.[26–28] Similarly, Ser83 binds to Gln116, which interacts with the guanine base, predicting indirect perturbation of nucleotide binding properties of CDC42. Cys81 is an invariant residue among RHO GTPases located in proximity of the phosphate-binding loop, and its substitution to phenylalanine was expected to cause favorable hydrophobic interactions with this loop, dislocation of Gly12, and consequently defective GTP hydrolysis. Finally, group III (CRIB mutations) included variants at Ile21, Tyr23, and Glu171, which are exposed residues predicted to affect interactions with effectors containing a CDC42/RAC-interacting binding (CRIB) motif (Figures 1B, 1C, and 1F).[29] Glu171 binds to Lys235 of WAS (WASP, hereafter) and plays a major role in the electrostatic binding network stabilizing the WASP-CDC42 association,[30,31] which was predicted to be disrupted by the Glu-to-Lys change. Tyr23 lies at the CDC42 surface implicated in PAK1 binding and stabilizes proper orientation of helix α5 mediating WASP binding.[32,33] Ile21 is located near the switch I region contributing to the hydrophobic pocket of helix α1 participating in WASP binding.[30] The Ile-to-Thr substitution was predicted to perturb CDC42 binding to signaling partners.

We assessed the effects of the disease-causing mutations on CDC42 GTPase activity, GDP/GTP exchange, and binding to effectors *in vitro*, using recombinant proteins. The p.Tyr23Cys, p.Tyr64Cys, p.Arg66Gly, p.Arg68Gln, p.Ser83Pro, p.Ala159Val, and p.Glu171Lys amino acid substitutions were selected as representative of the three mutation groups that were predicted to perturb differentially CDC42 function. pGEX vectors were used for bacterial overexpression of GST-tagged wild-type and mutant CDC42 proteins, and the GTPase-binding domains (GBD) of WASP (residues 154–321), PAK1 (residues 57–141), FMNL2 (residues 1–379), and IQGAP1 (residues 863–1657) in *E. coli* BL21 (DE3). Proteins were purified after cleavage of the GST tag (Superdex 75 or 200, GE Healthcare).[31] Nucleotide-free and fluorescent nucleotide-bound CDC42 variants were prepared using alkaline phosphatase

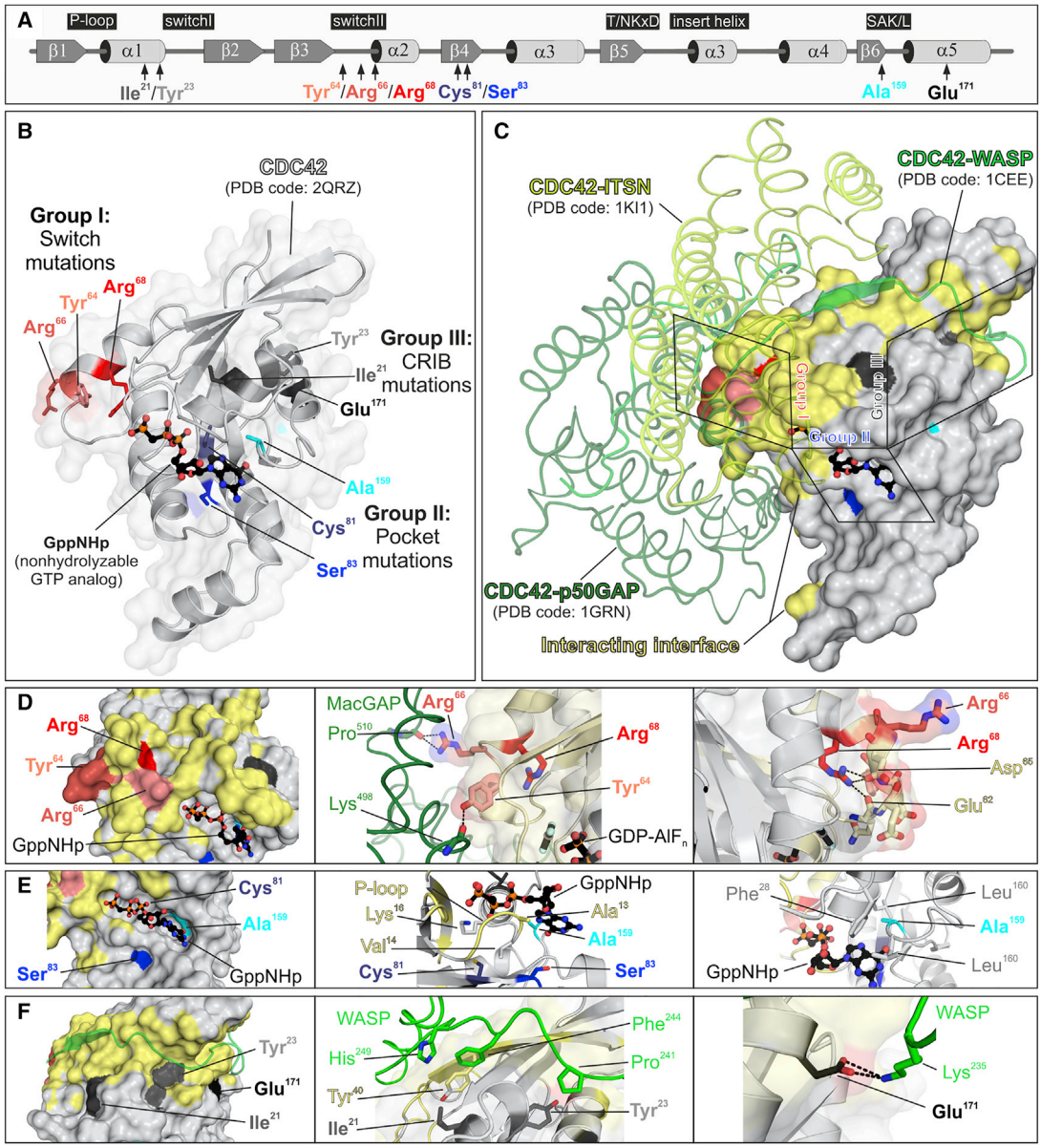

Figure 1. Location of Disease-Causing *CDC42* Mutations and Their Structural Impact

(A) Secondary structure elements (α helices and β strands), conserved motifs critical for tight guanine nucleotide binding and hydrolysis (G1–G5), and position of the identified disease-causing *CDC42* mutations are illustrated.

(B) Variant residues are assigned to three groups according to their position in the context of CDC42 structure (PDB: 2QRZ): group I or switch mutations (Tyr64, Arg66, and Arg68) are part of the switch II loop; group II or pocket mutations (Cys81, Ser83, and Ala159) are located in the vicinity of nucleotide binding pocket; and group III or CRIB mutations (Ile21, Tyr23, and Glu171) are far outside of the major interaction sites of CDC42 with GTP/GDP and involve exposed residues located in or close to regions of the protein mediating binding to effectors containing a CRIB motif.

(C) The position of the mutant residues relative to CDC42 interactions is illustrated by overlaying three different crystal structures of CDC42 in complex with ARHGAP1 ($p50^{GAP}$) (PDB: 1GRN), ITSN (PDB: 1KI1), and WAS (WASP) (PDB: 1CEE). Residues in reciprocal vicinity up to 4 Å were considered as part of binding interface. Residues of CDC42 mediating these interactions are shown in yellow.

(D) Group I mutations. Tyr64 and Arg66 are solvent-exposed residues and contribute to interactions with regulatory proteins and effectors (left). Interaction of both residues with ARHGAP18 (PDB: 5c2j) is shown as a representative for other interactions such as GEFs and effectors (middle). The disease-causing amino acid changes are predicted to affect this interaction. Arg68 participates in stabilizing the conformation of the switch II region via intramolecular interactions with Glu62 and Asp65 (right). The Arg-to-Gln change is predicted to destabilizes the switch II loop that is crucial for the interaction with signaling partners.

(E) Group II mutations. Cys81, Ser83, and Ala159 are in close vicinity of the phosphates (G1) and guanine base (G5) of bound GTP/GDP. Their substitutions are predicted to directly or indirectly affect the nucleotide binding affinity and to shift the balance between inactive and active CDC42 toward the latter.

(F) Group III mutations. Ile21, Tyr23, and Glu171 are part of a cavity on the CDC42 surface that accommodates the CRIB motif of bound effector proteins (e.g., WASP) (left). Ile21 and Tyr23 are critical for hydrophobic interactions (middle) with these type of proteins, while Glu171 contribute to binding mediating an electrostatic interaction (right).

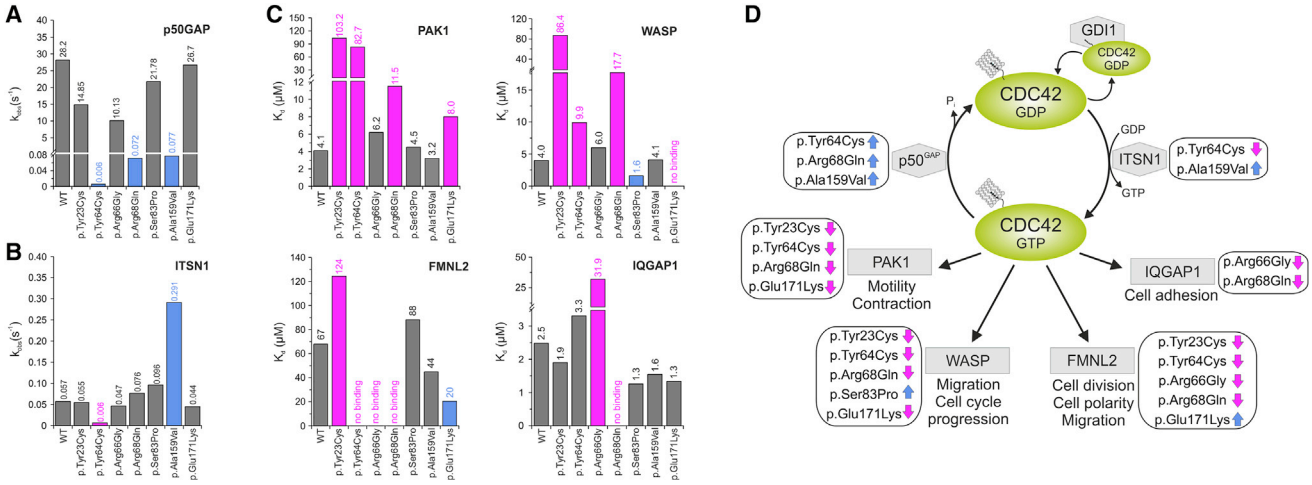

Figure 2. Assessment of the GTPase Activity, Nucleotide Exchange, and Binding to Effectors of Disease-Causing CDC42 Mutants
(A) Mean rate constants (k_{obs} values) of $p50^{GAP}$-stimulated GTP hydrolysis. Grey bars indicate non-significant differences compared to wild-type CDC42; blue bars indicate abolished/impaired GTP hydrolysis, which in turn results in an increased amount of active, GTP-bound CDC42 and thus enhanced signal flow. Data were obtained from >4 independent experiments.
(B) Mean rate constants (k_{obs} values) of the GEF-catalyzed release of labeled GDP (mantGDP). Grey bars indicate non-significant differences compared to wild-type CDC42; blue and magenta bars indicate increased or abolished nucleotide exchange, respectively. The former is predicted to promote enhanced signaling, while the latter blocks CDC42 in its inactive state. Data were obtained from >4 independent experiments.
(C) CDC42 mutants variably affect binding to effectors. Dissociation constants (K_d) obtained for the interaction of CDC42 proteins with PAK1, WASP, IQGAP1, and FMNL2 determined by fluorescence polarization. Data were collected from titration of increasing concentrations of the respective effectors. They were obtained from >4 independent experiments and are illustrated as bar charts. Grey bars indicate non-significant differences compared to wild-type CDC42; blue and magenta bars indicate increased or decreased binding affinity, respectively.
(D) Scheme summarizing the functional dysregulation of disease-causing mutants on downstream signaling pathways and cellular processes. ITSN1 is a specific GEF for CDC42 promoting the active state of the GTPase by catalyzing GDP release. $p50^{GAP}$ negatively controls CDC42 function by stimulating the GTP hydrolysis reaction. CDC42 interaction with PAK1, WASP, FMNL2, and IQGAP1 activates signaling pathways controlling different cellular processes. For each specific function, the blue and magenta arrows indicate the hyperactive or defective behavior, respectively.

(Roche) and phosphodiesterase (Sigma Aldrich) at 4°C.[31,34] First, GTPase activity was measured basally and following ARHGAP1 ($p50^{GAP}$, hereafter) stimulation by fluorescent experiments using tetramethylrhodamine (tamra-) GTP as substrate with a Hi-Tech Scientific (SF-61) stopped-flow instrument (Figures 2A and S2). The assays documented a variably increased basal GTP hydrolysis for $CDC42^{Tyr64Cys}$, $CDC42^{Arg68Gln}$, and $CDC42^{Ala159Val}$. Each of these mutants, however, exhibited robust GAP insensitivity, showing respectively a 4,700-fold ($CDC42^{Tyr64Cys}$), 392-fold ($CDC42^{Arg68Gln}$), and 366-fold ($CDC42^{Ala159Val}$) reduction in GAP-stimulated GTPase activity, compared to wild-type CDC42. A mildly decreased GAP-stimulated GTP hydrolysis was documented for $CDC42^{Tyr23Cys}$ and $CDC42^{Arg66Gly}$. By using the same experimental approach, release of methylanthraniloyl (mant-) GDP was used to assess the basal and GEF-catalyzed nucleotide exchange reactions (Figures 2B and S3). The assays documented an increase of GDP release for $CDC42^{Ala159Val}$ and a slightly increased nucleotide exchange for $CDC42^{Arg68Gln}$ and $CDC42^{Ser83Pro}$. By contrast, p.Tyr64Cys resulted in an almost completely abolished response to GEF. No substantial difference in GDP/GTP exchange behavior was observed for the other mutants. Then, fluorescence experiments were performed by using increasing amounts of the CDC42 interacting domains of WASP, PAK1, FMNL2, and IQGAP1 titrated to CDC42 proteins bound to mant-GppNHp, a non-hydrolyzable GTP analog, to assess the binding of mutants to four major CDC42 effectors and evaluate their ability to transduce signaling (Figures 2C and S4). Experiments were performed using a Fluoromax 4 fluorimeter in polarization mode, and the dissociation constants (K_d) were calculated by fitting the concentration-dependent binding curve using a quadratic ligand binding equation. Interaction with WASP was completely abolished in $CDC42^{Glu171Lys}$ and markedly decreased (21.6-fold) in $CDC42^{Tyr23Cys}$. Decreased binding, albeit to a milder degree, was documented for $CDC42^{Arg68Gln}$ and $CDC42^{Tyr64Cys}$, while $CDC42^{Ser83Pro}$ exhibited a slightly increased binding. Binding to PAK1 was impaired for $CDC42^{Tyr23Cys}$ and $CDC42^{Tyr64Cys}$ and reduced for $CDC42^{Arg68Gln}$ and $CDC42^{Glu171Lys}$. Tyr64 and Arg66 contribute to CDC42 binding to FMNL2;[35] consistently, $CDC42^{Tyr64Cys}$ and $CDC42^{Arg66Gly}$ had impaired FMNL2 binding, with the latter also having defective interaction with IQGAP1. Impaired binding to FMNL2 was also documented for $CDC42^{Tyr23Cys}$ and $CDC42^{Arg68Gln}$, the latter also exhibiting defective IQGAP1 binding. By contrast, $CDC42^{Glu171Lys}$ showed enhanced FMNL2 binding. Overall, biochemical characterization of CDC42

mutants confirmed the heterogeneous clinical and structural impact of variants demonstrating a stabilized GTP-bound conformation but defective interaction with all tested partners for group I mutations, variable hyperactive behavior for group II mutations, and a diversified binding to effectors for group III mutations (Figure 2D).

CDC42 is a master regulator of cell polarization and controls cell migration and growth.[36,37] The impact of CDC42 mutations on polarized migration was assessed by an *in vitro* wound-healing assay on fibronectin-coated wells (Sigma-Aldrich) (Figures 3A and S5). Monolayers of NIH 3T3 cells (American Type Culture Collection) cultured in high-glucose Dulbecco's modified Eagle's medium (DMEM) supplemented with 10% FCS, 2 mM L-glutamine, and 10 U/mL penicillin/streptomycin (Sigma-Aldrich) were transiently transfected using Fugene 6 (Roche) to express wild-type FLAG-tagged CDC42 isoform 1 (GenBank: NP_001782.1) or each of the p.Tyr23Cys, p.Arg68Gln, p.Ser83Pro, p.Ala159Val, and p.Glu171Lys mutants. 24 hr after transfection, cells were scratched and incubated in low serum medium in the presence of thymidine (Sigma-Aldrich) to inhibit cell proliferation. Cells that had migrated in the wounded area were counted 4 and 7 hr after scratch (four fields per well). Comparable transfection efficiency was verified by western blot analysis of the protein lysates. Only cells expressing group II mutants exhibited enhanced wound closure ability compared to cells expressing wild-type CDC42. Other tested mutants failed to increase migration, suggesting loss of function of this CDC42-mediated process, in line with defective binding of these mutants to WASP, a mediator of polarized migration.[38] Mutants also affected cell proliferation differentially (Figure 3A). $CDC42^{Ala159Val}$ and $CDC42^{Ser83Pro}$ variably enhanced cell growth, while $CDC42^{Tyr23Cys}$ and $CDC42^{Arg68Gln}$ significantly impaired proliferation, indicating a dominant-negative effect.

In *Caenorhabditis elegans*, CDC-42 controls early and late developmental programs (see WormBook in Web Resources), including vulval development,[39–41] a process that is regulated by LET-60/RAS-dependent and -independent signals.[42] To explore the impact of the disease-causing *CDC42* mutations *in vivo*, transgenic lines were generated to conditionally express wild-type CDC-42 or a selected subset of mutations for each mutation group (p.Tyr23Cys, p.Arg68Gln, p.Ser83Pro, p.Ala159Val, and p.Glu171Lys) affecting residues conserved in the nematode ortholog (Figure S6).[43] The wild-type *cdc-42* cDNA (ORF clone R07G3.1; ThermoScientific) was subcloned into the pPD49.83 heat shock-inducible vector (gift of A. Fire, Stanford University School of Medicine), and the generated constructs were injected at 100 ng/μL. The pJM67 plasmid (*pelt-2::NLS::GFP*) (gift from J.D. McGhee, University of Calgary), which drives green fluorescent protein (GFP) expression in intestinal cell nuclei, was used as co-injection marker (30 ng/μL). To analyze vulval induction and morphogenesis, synchronized animals from at least three independent lines for each construct were grown at 20°C and heat-shocked (90 min at 33°C followed by 30 min at 30°C) at late L2/early L3 larval stages and scored for vulval induction and morphogenesis from late L3 to mid L4 stages. The presence of a protruding vulva (Pvl phenotype), multiple ectopic pseudovulvae (multivulva [Muv] phenotype), and lack of a vulva (vulvaless [Vul] phenotype) was analyzed at the adult stage. Lines were scored in triplicate experiments using a Nikon Eclipse 80i instrument equipped with Nomarski differential interference contrast optics and used for further analyses and crosses. After each cross, the genotype of individual alleles was confirmed by direct sequencing of the appropriate genomic region. Isogenic animals that had lost the transgene were cloned separately and used as controls in each experiment. Overexpression of wild-type CDC-42 at the L2/L3 stage elicited a low-penetrant Muv phenotype, exacerbated the Muv phenotype associated with a *let-60* gain-of-function allele, *let-60*(*n1046*) *IV*, and partially rescued the Vul phenotype of animals carrying a hypomorphic *let-23/EGFR* allele, *let-23*(*sy1*) *II*, indicating LET-60/RAS signaling hyperactivation (Figures 3B and S7, Table S3). Compared to wild-type CDC-42, group II mutations induced a more severe Muv phenotype and more efficiently rescued the Vul phenotype of *let-23(sy1)* animals, indicative of enhanced signal flow through LET-60. Overexpression of wild-type CDC-42 also engendered aberrant vulva morphogenesis, generating a Pvl phenotype that was mediated, in part, by WSP-1/WASP (Figures 3B and S7, Tables S3 and S4). The same phenotype had previously been reported in *C. elegans* lines expressing the RASopathy-causing $SHOC2^{S2G}$ and $RRAS^{G39dup}$ mutants.[44,45] Like those animals, a variable proportion of CDC-42 hermaphrodites exhibiting Pvl displayed egg-laying defects (Egl phenotype) and accumulation of larvae inside the mother (Bag-of-worms phenotype) (data not shown). Of note, this phenotype was markedly promoted by group II mutations in a WASP-independent manner, indicating a gain-of-function effect of these changes. By contrast, $CDC\text{-}42^{Tyr23Cys}$, $CDC\text{-}42^{Arg68Gln}$, and $CDC\text{-}42^{Glu171Lys}$ significantly reduced the Pvl phenotype, supporting a selective hypomorphic behavior. Pvl was not modulated by *wsp-1* RNAi in animals expressing $CDC\text{-}42^{Tyr23Cys}$ and $CDC\text{-}42^{Glu171Lys}$ and was only slightly reduced in those expressing $CDC\text{-}42^{Arg68Gln}$, consistent with the biochemical data indicating an abolished or strongly reduced binding to WASP of those mutants, respectively. Nomarski observations of L3 and L4 control larvae showed that only P6.p descendants detached from the cuticle generating a single, symmetric invagination; by contrast, a variable proportion of larvae expressing wild-type and mutant CDC-42 displayed asymmetric and/or multiple invaginations (Figure S7), which represent the earliest signs of the Pvl and Muv phenotypes, respectively. Overall, the data indicate that group II mutations upregulate multiple signaling pathways, including LET-60/RAS, while the other variants behave as hypomorphic mutations on WASP-dependent signaling.

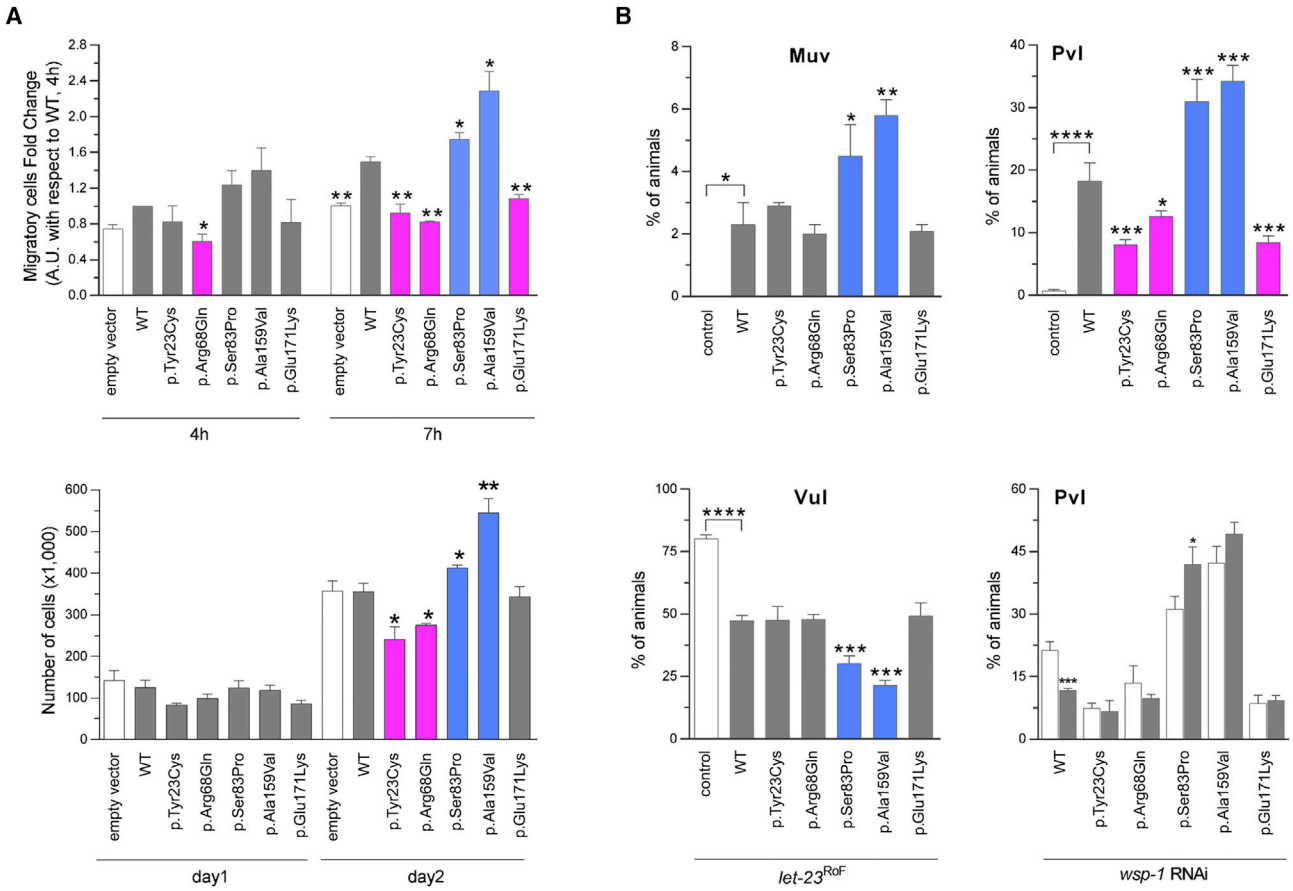

Figure 3. ***In Vitro* and *In Vivo* Functional Characterization of *CDC42* Mutations**

(A) *CDC42* mutations differentially impact polarized migration and cell proliferation. Wound-healing assays (above) and proliferation assays (below) were performed using NIH 3T3 cells transiently transfected to express wild-type CDC42 or each of the indicated mutants. Mean ± SD densitometry values of three independent experiments are shown. The wound was generated 24 hr after transfection, and migration in the wounded area was evaluated after 4 and 7 hr. Cells expressing exogenous wild-type CDC42 migrate more rapidly into the scratched area than cells transfected with the empty vector (EV). Mutants differentially perturb polarized migration, with $CDC42^{Ser83Pro}$ and $CDC42^{Ala159Val}$ overexpression variably enhancing the wound closure ability of transfected cells compared to the wild-type protein, whereas $CDC42^{Tyr23Cys}$, $CDC42^{Arg68Gln}$, and $CDC42^{Glu171Lys}$ fail to do that, supporting a gain-of-function and a loss-of-function effect of these mutants, respectively. Cell proliferation was evaluated in transfected cells at the indicated time points and quantified by manual counting using a Neubauer hemocytometer. The trypan blue dye exclusion test was used to consider viable cells only. While the $CDC42^{Ala159Val}$ and $CDC42^{Ser83Pro}$ mutants variably enhance proliferation compared to cells expressing wild-type CDC42, no effect on proliferation ($CDC42^{Glu171Lys}$) and reduced proliferation ($CDC42^{Tyr23Cys}$ and $CDC42^{Arg68Gln}$) is documented for the other mutants, indicating a loss-of-function and a dominant-negative effect, respectively. Asterisks indicate significant differences compared with wild-type CDC42 (*$p < 0.05$; **$p < 0.01$; Student's t test).

(B) Consequences of *CDC-42* expression on vulval development in *C. elegans*. Ectopic expression of wild-type CDC-42 at the L2/L3 stage elicits a multivulva (Muv) phenotype (left, upper panel), and CDC-42 overexpression in a LET-23/EGFR hypomorphic background reduces the penetrance of the vulvaless (Vul) phenotype (left, lower panel). Compared to animals expressing wild-type CDC-42, those expressing $CDC\text{-}42^{Ser83Pro}$ and $CDC\text{-}42^{Ala159Val}$ show higher prevalence of the Muv phenotype and lower prevalence of the Vul phenotype, indicating a gain-of-function role on LET-60/RAS signaling. Animals expressing the other tested CDC-42 mutants do not significantly differ from those expressing wild-type CDC-42. Ectopic expression of wild-type CDC-42 at the early L3 stage elicits a protruding vulva (Pvl) phenotype (right, upper panel). Animals expressing $CDC\text{-}42^{Ser83Pro}$ and $CDC\text{-}42^{Ala159Val}$ show a higher prevalence of the phenotype compared to worms expressing wild-type CDC-42, while a less penetrant phenotype was scored for animals expressing $CDC\text{-}42^{Tyr23Cys}$, $CDC\text{-}42^{Arg68Gln}$, or $CDC\text{-}42^{Glu171Lys}$ mutants. RNA interference (RNAi) experiments show that the Pvl phenotype associated with overexpression of wild-type CDC-42 is mediated, in part, by WSP-1/WASP (right, lower panel). White and gray bars indicate the penetrance of Pvl in non-interfered and interfered animals, respectively. Error bars indicate SEM of four independent experiments, and asterisks specify significance differences between animals expressing CDC-42 mutants and those expressing wild-type CDC-42 or between interfered and non-interfered nematodes (*$p < 0.05$; **$p < 0.001$; ***$p < 0.0001$; ****$p < 0.00005$; two-tailed Fisher's exact test). Comparisons between worms expressing wild-type CDC-42 and control animals are also shown. RNAi was performed by feeding using HT115 *E. coli* bacteria expressing double stranded *wsp-1* RNA (Ahringer's *C. elegans* RNAi feeding library) and optimized to overcome lethality. As a control of the efficiency of the modified RNAi protocol, *let-60* RNAi experiments were performed on animals carrying the *let-60* gain-of-function allele *n1046* (p.Gly13Glu), and the prevalence of the Muv phenotype was scored at a dissecting microscope (Table S4).

Figure 4. Facial Features of Individuals with Heterozygous *CDC42* Mutations
(A–C) Subject 3 (p.Tyr64Cys) at age 2 years and 6 months (A) and 15 years (B and C) showing upslanted palpebral fissures, smooth philtrum, flaring alae nasi, thin upper vermilion, and wide mouth with widely spaced teeth.
(D) Subject 4 (p.Arg66Gly) at 15 years showing broad forehead and broad nasal bridge with bulbous nasal tip.
(E and F) Subject 6 (p.Arg68Gln) at 24 months (E) and 4 years (F) showing a prominent broad forehead, hypertelorism, long philtrum, and thin upper vermilion.
(G and H) Subject 9 (p.Ser83Pro) at age 2 (G) and 6 (H) years showing prominent forehead, hypertelorism, wide mouth with cupid's bow, thin upper vermilion, and widely spaced teeth.
(I and J) Subject 10 (p.Ser83Pro) at 13 (I) and 32 (J) years showing prominent forehead, wide nasal bridge, ptosis, flared nostrils, and wide mouth with widely spaced teeth.
(K and L) Subject 11 (p.Ala159Val) at 2 years (K) and at 3 years and 7 months (L) showing very broad and prominent forehead, bulbous nasal tip, flared nostrils, cupid's bow, and downturned corners of the mouth.
(M–O) Subject 1 (p.Ile21Thr) at age 3 months (M), 2 years (N), and 10 years (O) showing synophrys, wide palpebral fissures, high and narrow nasal bridge, bulbous nasal tip, wide mouth with downturned corners, and mildly laterally prominent ears.
(P) Subject 2 (p.Tyr23Cys) at 14 years showing wide palpebral fissures, high nasal bridge with elevated nasal tip, short philtrum, and long neck.
(Q) Subject 12 (p.Glu171Lys) at 12 years showing typical facial features of Noonan syndrome, including broad forehead, hypertelorism, low-set ears, bulbous nasal tip, and flared nostrils.
(R) Subject 13 (p.Glu171Lys) showing ptosis, broad neck, and pectus deformity.
Note that individuals fitting the different mutation groups share some facial characteristics, and that intragroup variability is also observed.

The cohort of individuals carrying heterozygous mutations in *CDC42* had an unusually broad spectrum of anomalies. Core clinical features included defective growth, intellectual disability (ID), facial dysmorphism, hearing/vision problems, cardiac malformations, immune, hematologic, and lymphatic abnormalities, and brain malformations (Figures 4 and S8, Tables S5–S7, Supplemental Note). Correlating the functional impact of mutations on clinical phenotypes observed in affected individuals permitted a preliminary analysis of genotype-phenotype relationships (Table 2). Individuals with group I mutations manifested with ID, muscle tone abnormalities, and variable other less common features, including cardiac defects. All individuals within this group had thrombocytopenia, similar to two previously reported individuals.[20,21] Individuals with group II mutations manifested with strikingly dysmorphic facial features: subject 11 (p.Ala159Val) had marked hypertelorism, prominent forehead, bitemporal narrowing, and downslanting palpebral fissures with coarse thick hair, resembling a RASopathy (Figures 4K and 4L). Features within the Noonan syndrome phenotypic spectrum were observed in all affected individuals from two unrelated families carrying the c.511G>A (p.Glu171Lys) change (subjects 12 to 15), with

Table 2. Summary of the Clinical Features of *CDC42* Mutation-Positive Subjects

Mutation group	Group I	Group II	Group III
Number of individuals	5	4	6
Amino acid substitutions	p.Tyr64Cys, p.Arg66Gly, p.Arg68Gln	p.Cys81Phe, p.Ser83Pro, p.Ala159Val	p.Ile21Thr, p.Tyr23Cys, p.Glu171Lys
Growth			
Prenatal – weight at birth ≤ 2 SD	1/4	2/4	1/4
Prenatal – OFC at birth ≤ 2 SD	1/3	1/2	1/2
Postnatal – weight ≤ 2 SD	4/5	2/3	1/4
Postnatal – OFC ≤ 2 SD	3/5	2/4	3/4
Postnatal – growth deficiency	3/5	4/4	4/6
Intellectual disability	5/5	4/4	2/6
Seizures	1/4	2/4	1/6
MRI brain anomalies[a]	4/4	4/4	1/2
Tone anomalies	3/4	2/4	2/6
Optic atrophy	1/4	0/4	2/6
Endocrine anomalies	2/4	1/4	1/5
Facial dysmorphism[b]	4/5	4/4	6/6
Pectus deformity	1/5	0/4	4/5
Scoliosis/vertebral anomalies	2/5	1/4	2/6
Camptodacyly	1/5	2/4	1/5
Cardiac anomalies	3/5	2/4	2/5
GU anomalies	2/5	2/4	1/6
Lymphatic anomalies	1/5	1/4	0/6
Recurrent infections	4/5	3/4	1/6
Platelet anomalies (thrombocytopenia, macrothrombocytes)	4/4	1/3	0/5

Abbreviations: OFC, occipito-frontal circumference; SD, standard deviation; GU, genitourinary. Detailed phenotypic description of subjects is reported in the Supplemental Note and Table S5.
[a]For details regarding brain MRI features, see Figure S8 and Table S7.
[b]For details regarding the facial features, see Table S6.

a particularly striking gestalt of this disorder occurring in subject 12 (Figure 4Q). Notably, brain malformations occurred in all groups, and four individuals manifested with cerebellar-posterior fossa abnormalities. Subjects 8 and 11 (with group II mutations) had a large cerebellum with evidence of posterior fossa crowding and cerebellar tonsillar ectopia, features commonly reported in RASopathies.[46] It should be noted that notwithstanding the occurrence of a clinical overlap within each mutation group, intra-group phenotypic variability was observed, which would suggest a specific impact of individual mutations on developmental processes.

While traditionally CDC42 has been functionally linked to remodeling of the actin cytoskeletal architecture,[47] its role in controlling intracellular signaling has recently been broadened.[48] Such complex modulatory function is accomplished by interactions with a wide array of signaling partners functioning in distinct signal cascades. Cdc42 loss of function is embryonic lethal, and its targeted deletion has been shown to disrupt cell fate decision, differentiation, and function of multiple cell lineages as well as tissue homeostasis.[49] Here, we report that dominantly acting mutations differentially perturb CDC42 function and cause clinically heterogeneous phenotypes affecting development and growth. Group I mutations associated with impaired binding to regulators and effectors cause a syndromic form of thrombocytopenia, while the variably hyperactive group II mutations are associated with a variable developmental disorder characterized by striking dysmorphic features, and one specific amino acid change among the group III mutations, which affects only one of the two CDC42 isoforms and specifically impairs binding to WASP, results in an overall milder clinical phenotype that phenocopies Noonan syndrome.[14]

Noonan syndrome, the most common and clinically variable among the RASopathies, is caused by dysregulated signaling through RAS and the MAPK cascade. This disorder and its clinically related phenotypes result from

heterozygous germline mutations affecting *RAS* genes or genes coding proteins functioning as RAS effectors, regulators of RAS function, or more generally as modulators of RAS-MAPK signaling.[15] More recently, the family of genes implicated in RASopathies has been extended to include *LZTR1* (MIM: 600574), *RIT1* (MIM: 609591), and *RRAS* (MIM: 165090), which encode for signal transducers whose direct link to the RAS and the MAPK cascade had not previously been appreciated.[45,50,51] While it is possible that functional dysregulation of these proteins may impact RAS signaling directly or indirectly, these findings raise also the possibility that other pathways may contribute to disease pathogenesis. The present *in vivo* data provide evidence for enhanced signaling through RAS for group II mutations, indicating that upregulated CDC42 function is able to perturb signal flow through RAS; however, no effect on RAS-mediated signaling was inferred for the p.Glu171Lys change, here identified to be associated with a phenotype resembling Noonan syndrome. While it is possible that the used *in vivo* model failed in providing informative data for the specific effect of $CDC42^{Glu171Lys}$ on RAS signaling, our finding suggests that other processes, including aberrant cytoskeletal rearrangement, may represent a previously unappreciated aspect contributing to disease pathogenesis in Noonan syndrome. Consistent with this possibility, SOS1, SHOC2, and RRAS function has been linked to cell migration and other cellular processes strictly dependent on cytoskeletal rearrangement.[52–54] Further studies are thus required to specifically address the impact of dysregulated CDC42 function on RAS signaling as well as on the cellular and developmental processes that are altered in Noonan syndrome.

Overall, the present work links different classes of dominantly acting mutations of CDC42, a master regulator of actin cytoskeleton and major node in intracellular signaling, to a heterogeneous set of developmental and multi-system phenotypes, demonstrating the critical requirement of proper CDC42 function in a large array of developmental processes. This study also exemplifies current challenges in syndrome delineation in the post-WES era and emphasizes the relevance of functional profiling in syndrome recognition and delineation.

Accession Numbers

ClinVar accession ID for data provided herein are SCV000572034.2 (c.62T>C), SCV000244190.3 (c.68A>G), SCV000577577.2 (c.191A>G), SCV000244118.3 (c.196A>G), SCV000589746.1 (c.242G>T), SCV000678254 (c.203G>A), SCV000678255 (c.247T>C), SCV000678256 (c.476C>T), and SCV000678257 (c.511G>A).

Supplemental Data

Supplemental Data include a supplemental note (clinical data), eight figures, and seven tables and can be found with this article online at https://doi.org/10.1016/j.ajhg.2017.12.015.

Acknowledgments

We thank the families and referring physicians for their participation in this study. We thank Dr. David Wilson (Washington University, St. Louis) for providing clinical expertise and Dr. Serenella Venanzi (Istituto Superiore di Sanità, Rome) for technical assistance. This project was supported by the National Institute of Neurological Disorders and Stroke (NINDS) (K08NS092898 to G.M.M.), the Associazione Italiana per la Ricerca sul Cancro (AIRC) (IG17583 to M.T.), Fondazione Bambino Gesù (Vite Coraggiose to M.T.), Italian Ministry of Health (RF-2011-02349938 and Ricerca Corrente 2017 to M.T.), E-Rare (NSEuroNet to M.Z., M.R.A., and M.T.), International Research Training Group 1902 Intra- and Interorgan Communication of the Cardiovascular System (IRTG 1902 to E.A., M.B., and M.R.A.), and Medical Faculty of the Heinrich-Heine University Duesseldorf (9772617 to K.N., O.H.F.K., R.K., and M.R.A.). Exome sequencing was performed at the University of Washington Center for Mendelian Genomics (UW-CMG) and was funded by the National Human Genome Research Institute and the National Heart, Lung, and Blood Institute grant HG006493 (to D.A.N. and M.J.B.). This work was also supported by grants U01HL131003, UM1HL098147, UM1HL098123, UM1HL128761, UM1HL128711, and UM1HL098162 in support of the Pediatric Cardiac Genomics Consortium from the National Heart, Lung, and Blood Institute and the Eunice Kennedy Shriver National Institute of Child Health and Human Development. *C. elegans* strains were provided by the *Caenorhabditis* Genetics Center, which is funded by NIH Office of Research Infrastructure Programs (P40 OD010440). We also thank WormBase, the contributors to MyGene2, and the University of Washington Center for Mendelian Genomics for use of data.

Received: October 18, 2017
Accepted: December 18, 2017
Published: January 25, 2018

Web Resources

CADD, http://cadd.gs.washington.edu/
ClinVar, https://www.ncbi.nlm.nih.gov/clinvar/
dbNSFP, https://sites.google.com/site/jpopgen/dbNSFP
dbSNP, https://www.ncbi.nlm.nih.gov/projects/SNP/
ExAC Browser, http://exac.broadinstitute.org/
GenBank, https://www.ncbi.nlm.nih.gov/genbank/
gnomAD Browser, http://gnomad.broadinstitute.org/
NCBI Gene, https://www.ncbi.nlm.nih.gov/gene
OMIM, http://www.omim.org/
PyMOL, https://pymol.org/2
RCSB Protein Data Bank, http://www.rcsb.org/pdb/home/home.do
REVEL, https://sites.google.com/site/revelgenomics
WormBase, http://www.wormbase.org/
WormBook, http://www.wormbook.org

References

1. Bamshad, M.J., Ng, S.B., Bigham, A.W., Tabor, H.K., Emond, M.J., Nickerson, D.A., and Shendure, J. (2011). Exome sequencing as a tool for Mendelian disease gene discovery. Nat. Rev. Genet. *12*, 745–755.

2. Chong, J.X., Buckingham, K.J., Jhangiani, S.N., Boehm, C., Sobreira, N., Smith, J.D., Harrell, T.M., McMillin, M.J., Wiszniewski, W., Gambin, T., et al.; Centers for Mendelian Genomics (2015). The genetic basis of Mendelian phenotypes: discoveries, challenges, and opportunities. Am. J. Hum. Genet. *97*, 199–215.
3. Menke, L.A., van Belzen, M.J., Alders, M., Cristofoli, F., Ehmke, N., Fergelot, P., Foster, A., Gerkes, E.H., Hoffer, M.J., Horn, D., et al.; DDD Study (2016). CREBBP mutations in individuals without Rubinstein-Taybi syndrome phenotype. Am. J. Med. Genet. A. *170*, 2681–2693.
4. Lee, C.S., Fu, H., Baratang, N., Rousseau, J., Kumra, H., Sutton, V.R., Niceta, M., Ciolfi, A., Yamamoto, G., Bertola, D., et al.; Baylor-Hopkins Center for Mendelian Genomics (2017). Mutations in fibronectin cause a subtype of spondylometaphyseal dysplasia with "corner fractures". Am. J. Hum. Genet. *101*, 815–823.
5. Niceta, M., Stellacci, E., Gripp, K.W., Zampino, G., Kousi, M., Anselmi, M., Traversa, A., Ciolfi, A., Stabley, D., Bruselles, A., et al. (2015). Mutations impairing GSK3-mediated MAF phosphorylation cause cataract, deafness, intellectual disability, seizures, and a Down syndrome-like facies. Am. J. Hum. Genet. *96*, 816–825.
6. Reijnders, M.R.F., Ansor, N.M., Kousi, M., Yue, W.W., Tan, P.L., Clarkson, K., Clayton-Smith, J., Corning, K., Jones, J.R., Lam, W.W.K., et al.; Deciphering Developmental Disorders Study (2017). RAC1 missense mutations in developmental disorders with diverse phenotypes. Am. J. Hum. Genet. *101*, 466–477.
7. Martinelli, S., Torreri, P., Tinti, M., Stella, L., Bocchinfuso, G., Flex, E., Grottesi, A., Ceccarini, M., Palleschi, A., Cesareni, G., et al. (2008). Diverse driving forces underlie the invariant occurrence of the T42A, E139D, I282V and T468M SHP2 amino acid substitutions causing Noonan and LEOPARD syndromes. Hum. Mol. Genet. *17*, 2018–2029.
8. Philippakis, A.A., Azzariti, D.R., Beltran, S., Brookes, A.J., Brownstein, C.A., Brudno, M., Brunner, H.G., Buske, O.J., Carey, K., Doll, C., et al. (2015). The Matchmaker Exchange: a platform for rare disease gene discovery. Hum. Mutat. *36*, 915–921.
9. Sobreira, N., Schiettecatte, F., Valle, D., and Hamosh, A. (2015). GeneMatcher: a matching tool for connecting investigators with an interest in the same gene. Hum. Mutat. *36*, 928–930.
10. Chong, J.X., Yu, J.H., Lorentzen, P., Park, K.M., Jamal, S.M., Tabor, H.K., Rauch, A., Saenz, M.S., Boltshauser, E., Patterson, K.E., et al. (2016). Gene discovery for Mendelian conditions via social networking: de novo variants in KDM1A cause developmental delay and distinctive facial features. Genet. Med. *18*, 788–795.
11. Homsy, J., Zaidi, S., Shen, Y., Ware, J.S., Samocha, K.E., Karczewski, K.J., DePalma, S.R., McKean, D., Wakimoto, H., Gorham, J., et al. (2015). De novo mutations in congenital heart disease with neurodevelopmental and other congenital anomalies. Science *350*, 1262–1266.
12. Tanaka, A.J., Cho, M.T., Millan, F., Juusola, J., Retterer, K., Joshi, C., Niyazov, D., Garnica, A., Gratz, E., Deardorff, M., et al. (2015). Mutations in SPATA5 are associated with microcephaly, intellectual disability, seizures, and hearing loss. Am. J. Hum. Genet. *97*, 457–464.
13. Farwell Hagman, K.D., Shinde, D.N., Mroske, C., Smith, E., Radtke, K., Shahmirzadi, L., El-Khechen, D., Powis, Z., Chao, E.C., Alcaraz, W.A., et al. (2017). Candidate-gene criteria for clinical reporting: diagnostic exome sequencing identifies altered candidate genes among 8% of patients with undiagnosed diseases. Genet. Med. *19*, 224–235.
14. Roberts, A.E., Allanson, J.E., Tartaglia, M., and Gelb, B.D. (2013). Noonan syndrome. Lancet *381*, 333–342.
15. Tartaglia, M., and Gelb, B.D. (2010). Disorders of dysregulated signal traffic through the RAS-MAPK pathway: phenotypic spectrum and molecular mechanisms. Ann. N Y Acad. Sci. *1214*, 99–121.
16. Kircher, M., Witten, D.M., Jain, P., O'Roak, B.J., Cooper, G.M., and Shendure, J. (2014). A general framework for estimating the relative pathogenicity of human genetic variants. Nat. Genet. *46*, 310–315.
17. Dong, C., Wei, P., Jian, X., Gibbs, R., Boerwinkle, E., Wang, K., and Liu, X. (2015). Comparison and integration of deleteriousness prediction methods for nonsynonymous SNVs in whole exome sequencing studies. Hum. Mol. Genet. *24*, 2125–2137.
18. Ioannidis, N.M., Rothstein, J.H., Pejaver, V., Middha, S., McDonnell, S.K., Baheti, S., Musolf, A., Li, Q., Holzinger, E., Karyadi, D., et al. (2016). REVEL: an ensemble method for predicting the pathogenicity of rare missense variants. Am. J. Hum. Genet. *99*, 877–885.
19. Richards, S., Aziz, N., Bale, S., Bick, D., Das, S., Gastier-Foster, J., Grody, W.W., Hegde, M., Lyon, E., Spector, E., et al.; ACMG Laboratory Quality Assurance Committee (2015). Standards and guidelines for the interpretation of sequence variants: a joint consensus recommendation of the American College of Medical Genetics and Genomics and the Association for Molecular Pathology. Genet. Med. *17*, 405–424.
20. Takenouchi, T., Kosaki, R., Niizuma, T., Hata, K., and Kosaki, K. (2015). Macrothrombocytopenia and developmental delay with a de novo CDC42 mutation: Yet another locus for thrombocytopenia and developmental delay. Am. J. Med. Genet. A. *167A*, 2822–2825.
21. Takenouchi, T., Okamoto, N., Ida, S., Uehara, T., and Kosaki, K. (2016). Further evidence of a mutation in CDC42 as a cause of a recognizable syndromic form of thrombocytopenia. Am. J. Med. Genet. A. *170A*, 852–855.
22. Etienne-Manneville, S. (2004). Cdc42–the centre of polarity. J. Cell Sci. *117*, 1291–1300.
23. Heasman, S.J., and Ridley, A.J. (2008). Mammalian Rho GTPases: new insights into their functions from in vivo studies. Nat. Rev. Mol. Cell Biol. *9*, 690–701.
24. Colicelli, J. (2004). Human RAS superfamily proteins and related GTPases. Sci. STKE *2004*, RE13.
25. Dvorsky, R., and Ahmadian, M.R. (2004). Always look on the bright site of Rho: structural implications for a conserved intermolecular interface. EMBO Rep. *5*, 1130–1136.
26. Janakiraman, M., Vakiani, E., Zeng, Z., Pratilas, C.A., Taylor, B.S., Chitale, D., Halilovic, E., Wilson, M., Huberman, K., Ricarte Filho, J.C., et al. (2010). Genomic and biological characterization of exon 4 KRAS mutations in human cancer. Cancer Res. *70*, 5901–5911.
27. Gremer, L., Merbitz-Zahradnik, T., Dvorsky, R., Cirstea, I.C., Kratz, C.P., Zenker, M., Wittinghofer, A., and Ahmadian, M.R. (2011). Germline KRAS mutations cause aberrant biochemical and physical properties leading to developmental disorders. Hum. Mutat. *32*, 33–43.
28. Chang, M.T., Asthana, S., Gao, S.P., Lee, B.H., Chapman, J.S., Kandoth, C., Gao, J., Socci, N.D., Solit, D.B., Olshen, A.B.,

et al. (2016). Identifying recurrent mutations in cancer reveals widespread lineage diversity and mutational specificity. Nat. Biotechnol. *34*, 155–163.
29. Pirone, D.M., Carter, D.E., and Burbelo, P.D. (2001). Evolutionary expansion of CRIB-containing Cdc42 effector proteins. Trends Genet. *17*, 370–373.
30. Abdul-Manan, N., Aghazadeh, B., Liu, G.A., Majumdar, A., Ouerfelli, O., Siminovitch, K.A., and Rosen, M.K. (1999). Structure of Cdc42 in complex with the GTPase-binding domain of the 'Wiskott-Aldrich syndrome' protein. Nature *399*, 379–383.
31. Hemsath, L., Dvorsky, R., Fiegen, D., Carlier, M.F., and Ahmadian, M.R. (2005). An electrostatic steering mechanism of Cdc42 recognition by Wiskott-Aldrich syndrome proteins. Mol. Cell *20*, 313–324.
32. Morreale, A., Venkatesan, M., Mott, H.R., Owen, D., Nietlispach, D., Lowe, P.N., and Laue, E.D. (2000). Structure of Cdc42 bound to the GTPase binding domain of PAK. Nat. Struct. Biol. *7*, 384–388.
33. Gizachew, D., Guo, W., Chohan, K.K., Sutcliffe, M.J., and Oswald, R.E. (2000). Structure of the complex of Cdc42Hs with a peptide derived from P-21 activated kinase. Biochemistry *39*, 3963–3971.
34. Hemsath, L., and Ahmadian, M.R. (2005). Fluorescence approaches for monitoring interactions of Rho GTPases with nucleotides, regulators, and effectors. Methods *37*, 173–182.
35. Kühn, S., Erdmann, C., Kage, F., Block, J., Schwenkmezger, L., Steffen, A., Rottner, K., and Geyer, M. (2015). The structure of FMNL2-Cdc42 yields insights into the mechanism of lamellipodia and filopodia formation. Nat. Commun. *6*, 7088.
36. Melendez, J., Liu, M., Sampson, L., Akunuru, S., Han, X., Vallance, J., Witte, D., Shroyer, N., and Zheng, Y. (2013). Cdc42 coordinates proliferation, polarity, migration, and differentiation of small intestinal epithelial cells in mice. Gastroenterology *145*, 808–819.
37. Zegers, M.M., and Friedl, P. (2014). Rho GTPases in collective cell migration. Small GTPases *5*, e28997.
38. Beaty, B.T., and Condeelis, J. (2014). Digging a little deeper: the stages of invadopodium formation and maturation. Eur. J. Cell Biol. *93*, 438–444.
39. Welchman, D.P., Mathies, L.D., and Ahringer, J. (2007). Similar requirements for CDC-42 and the PAR-3/PAR-6/PKC-3 complex in diverse cell types. Dev. Biol. *305*, 347–357.
40. Lohmer, L.L., Clay, M.R., Naegeli, K.M., Chi, Q., Ziel, J.W., Hagedorn, E.J., Park, J.E., Jayadev, R., and Sherwood, D.R. (2016). A sensitized screen for genes promoting invadopodia function in vivo: CDC-42 and Rab GDI-1 direct distinct aspects of invadopodia formation. PLoS Genet. *12*, e1005786.
41. Choi, M.S., Yoo, A.S., and Greenwald, I. (2010). sel-11 and cdc-42, two negative modulators of LIN-12/Notch activity in *C. elegans*. PLoS ONE *5*, e11885.
42. Schmid, T., and Hajnal, A. (2015). Signal transduction during *C. elegans* vulval development: a NeverEnding story. Curr. Opin. Genet. Dev. *32*, 1–9.
43. Mello, C.C., Kramer, J.M., Stinchcomb, D., and Ambros, V. (1991). Efficient gene transfer in *C.elegans*: extrachromosomal maintenance and integration of transforming sequences. EMBO J. *10*, 3959–3970.
44. Cordeddu, V., Di Schiavi, E., Pennacchio, L.A., Ma'ayan, A., Sarkozy, A., Fodale, V., Cecchetti, S., Cardinale, A., Martin, J., Schackwitz, W., et al. (2009). Mutation of SHOC2 promotes aberrant protein N-myristoylation and causes Noonan-like syndrome with loose anagen hair. Nat. Genet. *41*, 1022–1026.
45. Flex, E., Jaiswal, M., Pantaleoni, F., Martinelli, S., Strullu, M., Fansa, E.K., Caye, A., De Luca, A., Lepri, F., Dvorsky, R., et al. (2014). Activating mutations in RRAS underlie a phenotype within the RASopathy spectrum and contribute to leukaemogenesis. Hum. Mol. Genet. *23*, 4315–4327.
46. Gripp, K.W., Hopkins, E., Doyle, D., and Dobyns, W.B. (2010). High incidence of progressive postnatal cerebellar enlargement in Costello syndrome: brain overgrowth associated with HRAS mutations as the likely cause of structural brain and spinal cord abnormalities. Am. J. Med. Genet. A. *152A*, 1161–1168.
47. Nobes, C.D., and Hall, A. (1995). Rho, rac and cdc42 GTPases: regulators of actin structures, cell adhesion and motility. Biochem. Soc. Trans. *23*, 456–459.
48. Arias-Romero, L.E., and Chernoff, J. (2013). Targeting Cdc42 in cancer. Expert Opin. Ther. Targets *17*, 1263–1273.
49. Pedersen, E., and Brakebusch, C. (2012). Rho GTPase function in development: how in vivo models change our view. Exp. Cell Res. *318*, 1779–1787.
50. Aoki, Y., Niihori, T., Banjo, T., Okamoto, N., Mizuno, S., Kurosawa, K., Ogata, T., Takada, F., Yano, M., Ando, T., et al. (2013). Gain-of-function mutations in RIT1 cause Noonan syndrome, a RAS/MAPK pathway syndrome. Am. J. Hum. Genet. *93*, 173–180.
51. Yamamoto, G.L., Aguena, M., Gos, M., Hung, C., Pilch, J., Fahiminiya, S., Abramowicz, A., Cristian, I., Buscarilli, M., Naslavsky, M.S., et al. (2015). Rare variants in SOS2 and LZTR1 are associated with Noonan syndrome. J. Med. Genet. *52*, 413–421.
52. Sini, P., Cannas, A., Koleske, A.J., Di Fiore, P.P., and Scita, G. (2004). Abl-dependent tyrosine phosphorylation of Sos-1 mediates growth-factor-induced Rac activation. Nat. Cell Biol. *6*, 268–274.
53. Holly, S.P., Larson, M.K., and Parise, L.V. (2005). The unique N-terminus of R-ras is required for Rac activation and precise regulation of cell migration. Mol. Biol. Cell *16*, 2458–2469.
54. Kaduwal, S., Jeong, W.J., Park, J.C., Lee, K.H., Lee, Y.M., Jeon, S.H., Lim, Y.B., Min, S., and Choi, K.Y. (2015). Sur8/Shoc2 promotes cell motility and metastasis through activation of Ras-PI3K signaling. Oncotarget *6*, 33091–33105.

The American Journal of Human Genetics, Volume *102*

Supplemental Data

Functional Dysregulation of CDC42

Causes Diverse Developmental Phenotypes

Simone Martinelli, Oliver H.F. Krumbach, Francesca Pantaleoni, Simona Coppola, Ehsan Amin, Luca Pannone, Kazem Nouri, Luciapia Farina, Radovan Dvorsky, Francesca Lepri, Marcel Buchholzer, Raphael Konopatzki, Laurence Walsh, Katelyn Payne, Mary Ella Pierpont, Samantha Schrier Vergano, Katherine G. Langley, Douglas Larsen, Kelly D. Farwell, Sha Tang, Cameron Mroske, Ivan Gallotta, Elia Di Schiavi, Matteo della Monica, Licia Lugli, Cesare Rossi, Marco Seri, Guido Cocchi, Lindsay Henderson, Berivan Baskin, Mariëlle Alders, Roberto Mendoza-Londono, Lucie Dupuis, Deborah A. Nickerson, Jessica X. Chong, The University of Washington Center for Mendelian Genomics, Naomi Meeks, Kathleen Brown, Tahnee Causey, Megan T. Cho, Stephanie Demuth, Maria Cristina Digilio, Bruce D. Gelb, Michael J. Bamshad, Martin Zenker, Mohammad Reza Ahmadian, Raoul C. Hennekam, Marco Tartaglia, and Ghayda M. Mirzaa

SUPPLEMENTAL DATA

TABLE OF CONTENTS

SUPPLEMENTAL CLINICAL DATA

Subject 1 (LR16-483; p.Ile21Thr)

This African American male was born to healthy, non-consanguineous parents. He has a healthy older brother. He was born at 35 weeks of gestation and was hospitalized for three weeks because of feeding issues, poor suck, and respiratory difficulties. He was referred to Genetics at age 5 months due to three failed hearing screens and mild dysmorphic facial features including a prominent forehead, a high and narrow nasal bridge, broad nasal tip, apparent synophrys with prominent metopic sutures. At that time, he was noted to have some developmental delays. His head growth began to decrease starting at age 1 month. He underwent release of his tethered cord (just below L2) at age 16 months. He also has a history of equinus deformity of the left foot. He was diagnosed with unilateral renal agenesis following frequent urinary tract infections. He did not speak until almost age 2 years, requiring speech therapy through elementary school. He had inguinal hernia repair and urethral repair with orchidoplasty at age 6 years. He also has a diagnosis of attention-deficit hyperactivity disorder (ADHD) requiring medication. He had scoliosis and was followed by orthopedic surgery. He was evaluated by hematology and oncology specialists in 2017 following a complete blood count (CBC) that showed a total white blood cell (WBC) count of 1,900/mm^3 with an absolute neutrophil count (ANC) of 600/mm^3 and platelets of 143,000/mm^3. A recheck noted his total WBC count was up to 2.9 K/mm^3, his ANC was 900 and his platelets were 270. Brain MRI performed at 13 months was normal. Previous normal genetic tests included chromosomes, subtelomeric FISH, and SNP chromosomal microarray.

Subject 2 (LR14-224; p.Tyr23Cys)

This child's family consisted of healthy parents, two male children and one female child. The proband was 4 years of age at time of referral and presented with severe intellectual deficiency (ID), growth failure, autistic features, microcephaly, seizures, absent speech, and dysmorphic facial features including unilateral ptosis, up-turned nasal tip, short philtrum, and long neck. Developmentally, he gained head control at age 4 to 6 months, sat independently at 9 months, and walked at 24 months of age. He began having seizures at 5 months of age. He has been diagnosed with secondary generalized epilepsy with multiple seizure types. His seizures have been medically refractory. At his most recent visit at age 17 years, his seizures were relatively under good control with zonisamide and lacosamide. He remained nonverbal, but he can follow commands and answer questions by signing. Brain MRI performed at 1 years showed diffuse cerebral and cerebellar atrophy, mild cerebellar vermis hypoplasia, ventriculomegelay and thin corpus callosum. Extensive biochemical and genetic testing failed to identify an underlying disease etiology including chromosome analysis, subtelomeric FISH, CGH/SNP microarray, methylation testing for Angelman/Prader Willi syndrome and uniparental disomy, *MECP2*, *CDKL5*, *FOXG1*, *ARX* sequencing, a 90 gene X-linked intellectual disability gene panel, a 53-gene seizure panel, and a 101 nuclear mitochondrial gene panel, in addition to several biochemical tests, all of which were inconclusive.

Subject 3 (LR17-420; p.Tyr64Cys)

The proband is a 15-year-old female followed since birth by the Genetics service at the Hospital for the Sick Children. She is the only child of a 32-year-old mother of Filipino descent and a 60-year-old father of English descent. She was born at 41 weeks by spontaneous vaginal delivery after an uneventful pregnancy. Apgar scores were 5 at 1 minute and 7 at 5 minutes, respectively. Birth weight was 2.44 kg (–2 SD below the mean), length 50 cm (50^{th} centile) and occipito-frontal circumference (OFC) 32 cm (–2.2 SD below the mean). She had dysmorphic features including hypertelorism, low-set ears, upslanting palpebral fissures, medially-flared eyebrows and small chin,

in addition to distal arthrogryposis. She also had a two-vessel cord. She developed cyanosis and was admitted to the Neonatal Intensive Care Unit at birth. She was ventilated for 2 days. Echocardiogram showed ventricular septal defect (VSD), patent ductus arteriosus (PDA) and atrial septal defect (ASD). The ASD and VSD were repaired at age of 15 months, and the PDA closed spontaneously. Head ultrasound showed no major structural anomalies. She had feeding problems from birth that required nasogastric tube feeds. A G-tube was placed for severe gastro-esophageal reflux disease (GERD) at 4 months of age, and was required until the patient was 6 years old. She had persistent constipation that is still managed with PEG flakes. At age 8 months, ABR confirmed profound hearing loss on the right side and significant partial loss on the left side. At age 13 months, she was diagnosed with myxedema secondary to severe hypothyroidism, which has since been treated. Renal ultrasound showed mild bilateral pelviectasis. At age 3.5 years, the child underwent bilateral inguinal hernia repair. History is also remarkable for multiple allergies to medications and recurrent infections, including multiple viral and respiratory infections and bacteremia with low B-cell and T-cell counts, as well as low immunoglobulins. She has intermittent thrombocytopenia and neutropenia, asthma, and eczema. She has not experienced any significant infections since prophylactic amoxicillin was initiated at age 12 years. Examination of the limbs revealed limitations of the proximal interphalangeal (PIP) and distal interphalangeal (DIP) joints in both hands with left index finger being most severely affected. The fingers were also noted to be tapered and slender. In the lower limbs, the right 4th digit was noted to be proximally inserted. The range of movement of the large joints was within normal limits. She also had truncal hypotonia, with normal patellar reflexes.

The subject developed more significant camptodactyly over time. At the last examination, at age 15 years, her dysmorphic facial features had become more obvious. She had upslanting palpebral fissures, small and thin nose, flat philtrum, thin upper lip with downturned corners of the mouth, prominent glabella and small ears. From a developmental standpoint, she had global developmental delay. She walked with support at age 2.5 years. At 15 years of age, she could walk independently, but had an unstable wide-based gait and triped easily. She has remained without intelligible words, but learned to communicate with a private repertoire of gestures. She does not write or read, but used an I-pad with a Pro Logic II program for general communication primarily at school and at home, due to anxiety in other settings. She is partially toilet trained. With regards to other systems, fundus examination was grossly normal, although the optic nerves were noted to be somewhat pale with possible subtle nerve fiber layer loss. Abdominal ultrasound in the neonatal period showed a Superior Mesenteric Vein (SMV) directly anterior to the Superior Mesenteric Artery (SMA). She had a normal IGF1 of 147 μg/L at age 7 years. Spinal radiographs demonstrated subtle scoliosis measuring 14 degrees, and a 67 degree kyphosis measured between T5 and12.

Subject 4 (LR14-352; p.Arg66Gly)

This family consisted of the proband, parents and five older siblings. The proband was a 16-year-old male with a complex medical history characterized by multi-system involvement including intrauterine growth retardation, growth hormone deficiency, precocious puberty, and immunodeficiency (hypogammaglobulinemia associated with multiple infections). He received Intravenous Immunoglobulin (IVIG) in several forms with a reduction in the frequency of infections. The subject also has multiple vertebral anomalies, spinal fusion and kyphosis, widened central spinal canal, abnormal renal vascular system (4 renal arteries on the right and 3 renal arteries on the left), severe progressive hearing loss, hyperopia with anomalous optic nerves and thick corneas, annular pancreas, dysmorphic facial features (broad forehead, bilateral ptosis, a high, narrow nasal bridge with a broad nasal tip, wide mouth and widely spaced teeth), submucous cleft palate, syndactyly of the hands and feet (consists of 3-4 syndactyly of the left hand and 2-3 syndactyly of both feet), peg-like teeth (suggestive of ectodermal dysplasia), Legg-Calve-Perthes

disease of the right hip, multiple dysplastic skin moles, history of chronic loose bowel movements, chordee, learning disability, and developmental delay.

At the time of this report (18 year-old), the subject had undergone 39 surgeries including gastrostomy (G-) tube placement, annular pancreas repair, pericardial effusion that required pericardiectomy, cochlear implant placement, syndactyly and cleft palate repair, hemi-laminectomy at L1-L2 vertebral levels, bilateral decompression at L3-L4, bilateral proximal femoral and distal femoral extension osteotomies, and tibial de-rotation. He has intermittent treatment for hypertension, and has multiple joint contractures. Magnetic Resonance Imaging (MRI) of the brain showed abnormal signals in the periventricular white matter suggestive of dysmyelination. Renal computed tomography (CT) and angiography revealed multiple small renal arteries. Further testing revealed that Factor 13, Subunit A antigen levels were low. He underwent the following tests, which were inconclusive: karyotypes of blood and skin, telomeric FISH, array CGH, *TP63* sequence analysis, urine mucopolysaccharide (MPS) and oligosaccharide levels, and Factor 8 and Von Willebrand antigen levels.

Of his five siblings, one brother has pectus excavatum and a history of abnormal moles, another was born with a submucous cleft, and one sister had 3 pilonidal cysts, which were surgically-removed. The proband has several cousins who also presented with developmental problems, including two males with Asperger Syndrome and one male with pilonidal cysts (children of proband's 1st maternal uncle), one female with scoliosis (daughter of proband's 2nd maternal uncle), one female with an open fistula at the base of her neck (daughter of proband's maternal aunt), and one female who suffered sudden death at age 14 due to seizure (daughter of proband's paternal aunt).

Subject 5 (PCGC 1-04248; p.Arg66Gly)

This individual is a Caucasian-of-European-descent female infant who was born to healthy non-consanguineous parents. The mother was age 28.4 years and the father was 27.1 years at the time of delivery. This infant was born with aortic coarctation with stenosis of the left coronary artery ostium and bilateral pulmonary branch stenosis. Medical history is also remarkable for failure to thrive, mild developmental delays, and decreased hearing. This individual died around age 8 months due to cardiovascular complications, with otherwise limited medical data.

Subject 6 (ISS3MO; p.Arg68Gln)

This boy was born to healthy non-consanguineous parents. Mother was 35 years and father 40 years at the time of delivery. The child was born prematurely at 27 weeks of gestation. Birth weight was 965 grams (50^{th} percentile for gender and gestational age), length 32 cm (6^{th} percentile for gender and gestational age), and OFC 25 cm (–0.25 SD for gender and gestational age). He had a history of poor sucking and swallowing. His growth measurements on last assessment at age 4 years were 13 Kg ($<3^{rd}$ centile, –2.4 SD), length 93 cm ($<3^{rd}$ centile, –2.29 SD) and OFC 49 cm ($<3^{rd}$ percentile). He had several dysmorphic facial features including sparse hair with whorls, prominent forehead, epicanthal folds, wide nasal bridge, flared nostrils with a broad nasal tip, long philtrum, an under-developed midface, thick ears and a webbed appearance of the neck. He had sensorineural hearing loss, with a 50-70 DB threshold. Developmentally, he had cognitive deficits. His Griffiths developmental quotient was 70 at 24 months. He also had a history of hypertrophic cardiomyopathy, thrombocytopenia, elbow and arm contractures. He had a recurrent maculopapular cutaneous eruption, gastrointestinal bleeding episodes, recurrent fever, as well as polyserositis (pleural, pericardial effusion and ascites). He also had splenomegaly. His brain MRI showed mildly prominent periventricular white matter signal intensities (predominantly posteriorly), ventriculomegaly and increased extra-axial space. Previously performed genetic testes included an array CGH which revealed a paternally-inherited 716Kb deletion of 14q13.1, as well as sequencing

of the *PTPN11, SOS1, RAF1, KRAS, BRAF, MEK1, MEK2, HRAS, NRAS,* and *SHOC2* genes, which were all normal.

Subject 7 (ISS4BO; p.Arg68Gln)

This girl was born at term (at a gestational age of 39 weeks and two days) to healthy non-consanguineous parents. Birth weight was 3455 grams (0 SD), length 47 cm (25th centile) and OFC 36 cm (+1.5 SD). Apgar scores were 8, 9 at 1, 5 minutes, respectively She was 5 years-old at the time of the last clinical evaluation and growth measurements were the following: weight 15.5 Kg (3-10th centile), length 101 cm (3-10th centile), OFC 51 cm (+0.25 SD). Facial examination showed several dysmorphic facial features including spare hair and eyebrows, broad, prominent forehead, wide nasal bridge, long philtrum, underdeveloped mid-face, cubid's bow and low-set ears. A ventricular septal defect (VSD) was detected prenatally and confirmed at birth. Surgical correction was undertaken at the age of 3 years. She also had bilateral inguinal hernia that was treated surgically at the age of six months. She presented with early-onset thrombocytopenia, with a platelet count of 19,000-69,000/mmc, with occasional giant platelets identified by blood smear analysis, associated with macrocytic anemia. She also had sensorineural deafness with a 60-70 DB threshold. Developmentally, the child had global developmental delay. She could walk unassisted at age 30 months. However, language of the child continued to be non-verbal at last clinical evaluation. She had febrile seizures, with four reported seizure episodes. Brain MRI showed partial agenesis of the corpus callosum and sub-ependymal heterotopia.

Subject 8 (LR17-032; p.Cys81Phe)

The subject is a 4-year-old boy born to healthy, non-consanguineous parents. He has a healthy and developmentally-normal older brother. He was born at 38 weeks of gestation. Birth weight was 2.89 Kg (10-25th percentile), and length 45.7 cm (–2 SD). The child had a history of recurrent infections, gastroesophageal reflux disease, speech delays and microcephaly. He also has ptosis, strabismus, dysmorphic facial features (including wide palpebral fissures, up-turned nasal tip, flattened nasal bridge, thin upper lip, long philtrum, down turned corners of the mouth, low-set ears), and webbing of the penis. His growth had been consistently tracking below the 5th percentile. Vision and hearing were normal. Developmentally, he had speech delays, with velopharyngeal insufficiency for which a pharyngeal flap repair has been recommended. Otherwise, his cognitive development was assessed to be age-appropriate at age 4 years. Brain MRI showed prominent perivascular spaces throughout the deep white matter and basal ganglia, mild thinning of the corpus callosum and mega cisterna magna.

Subject 9 (LR10-046; p.Ser83Pro)

This boy was born to healthy non-consanguineous parents. He was conceived by In Vitro Fertilization (IVF). He had several complex medical issues. He was noted to have hydrocephalus with ventriculomegaly on early brain MRI scans and underwent ventriculoperitoneal (VP) shunt placement at 8 months of age. He had several dysmorphic facial features including a broad, prominent forehead, wide nasal bridge, long philtrum, cubid's bow, broad jaw, and widely-spaced teeth. Ventriculomegaly resolved after shunting. He also had congenital heart disease including total anomalous pulmonary venous return (TAPVR) and coarctation of the aorta status post-surgical correction. He was formally diagnosed with growth hormone deficiency, short stature and hypothyroidism. He was noted to have anhidrosis and easily became hyperthermic. Spinal imaging showed a tethered cord with the conus ending at L2-L3 level, as well as a syrinx extending from T2-L1. He had recurrent respiratory infections including several episodes of pneumonias, with no evidence of immunodeficiency. He also has recurrent asthma. Other medical issues include

strabismus that was surgically repaired, scoliosis, epilepsy, intellectual disability, and Autism Spectrum Disorder (ASD).

Subject 10 (LR16-056; p.Ser83Pro)

The proband is a 34-year-old male who was born to 34-year-old mother and 37-year-old father. Birth weight was 3270 grams (–0.5 SD) and length was 49.5 cm (~0 SD). He had several dysmorphic facial features that evolved over time including spare hair, prominent forehead, hypertelorism, bilateral ptosis, wide nasal bridge, flared nostrils, wide mouth with widely-spaced teeth. He had history of congenital lymphedema that has persisted throughout his life, a history of meningitis at age 4 months, and frequent episodes of cellulitis in lymphedematous legs. Recurrent infections subsided around adolescence. He had a history of myoclonic seizures during infancy and later in puberty. His growth measurements at age 34 years were the following: weight 70 Kg, and height 161 cm (–2.5 SD). He had mild developmental delays. He had good verbal language development but poor overall developmental functioning, and poor visual memory. Brain MRI at age 34 years showed ventriculomegaly and cerebellar tonsillar ectopia.

Subject 11 (LR15-338; p.Ala159Val)

This 7 year-old proband was the product of a 38-week gestation to 26-year-old G4, P0-1 mother. Pregnancy was complicated by a concern for a Dandy-Walker malformation on prenatal ultrasound and a single umbilical artery. Amniocentesis demonstrated a normal 46,XY karyotype. Apgar scores after birth were 9 and 9 at 1 and 5 minutes, respectively. His birthweight was 2.49 Kg (–2 SD), length 45 cm (–2 SD), and head circumference 31 cm (–3 SD). The diagnosis of a Dandy-Walker malformation was confirmed through a postnatal CT scan which also showed dysgenesis of the corpus callosum. Brain MRI was markedly abnormal and showed wide-spread white matter signal intensities, partial agenesis of the corpus callosum, and marked abnormalities of the cerebellum, brainstem and hippocampus. He had diffuse cerebellar foliar dysplasia with a large inferior cerebellar peduncle, small middle cerebellar peduncle, and stretched superior cerebellar peduncle. The cerebellar vermis was small and uprotated, consistent with a Dandy-Walker malformation. The thalami were small, along with the medulla and pons, with a cleft in the tectum. The hippocampus was unilaterally dysplastic as well. A renal ultrasound was also obtained and showed hydronephrosis. Physical examination at the time also demonstrated hypospadias, undescended testes, and a dilated left pupil on ocular exam. He was subsequently transferred to a nearby Children's Hospital for further evaluation and was discharged from the neonatal intensive care unit (NICU) there at 2 weeks of age. He followed with nephrology for asymmetric kidney size with poor corticomedullary differentiation and pelviectasis. He was also diagnosed with cerebral palsy and seizures. He followed up with ophthalmology for oculomotor nerve palsy and required glasses for strabismus. Developmentally, the proband rolled over between 6-8 months of age, sat at 24 months, and began crawling and pulling to stand at 4.5 years of age. He continued to be non-verbal, using signs and an augmented communication device in the school setting.

On physical exam at 6 years of age, the proband’s weight was 16.2 kg (–2 SD), height 97cm (–4 SD), and OFC was 47.8cm (–3 SD). He was found to be grossly microcephalic with frontal bossing, bitemporal narrowing and prominence of the parietal areas of his skull. He also had prominent metopic suture and supraorbital ridges. He had widely set eyes with sparse hair and eyebrows, bilateral ptosis, flattened midface, broad nasal root, normally formed philtrum and a slightly tented upper lip. Ears were slightly posteriorly rotated with prominent lobes. His upper dentition appeared normal. He had bilateral ptosis, (left greater than right) with exotropia. Hands showed bilateral clinodactyly, proximally placed thumbs, and tapering of his fingers. Feet showed overlap of his great and third toes over the second toe.

Subject 12 (M060721; p.Glu171Lys)

The male proband is the first child to healthy unrelated parents, with a younger healthy brother. At birth, the mother was 29 years old and the father 34 years old. The child was born by vaginal delivery at term following an uneventful pregnancy. Birth weight was 3170 grams (–1.5 SD), length 50 cm (0 SD), and OFC 34 cm (–1 SD). Apgar scores were 8 and 9 at 1 and 5 minutes, respectively. He was first evaluated by genetics at the age of 7 years. Weight was 26 kg (75^{th}-90^{th} centile), height 118 cm (25^{th}-50^{th} centile), OFC 50 cm (10^{th} centile). Physical examination showed microdolicocephalic skull, curly hair, bi-temporal constriction with mild prominence of the metopic suture, sparse hair and eyebrows, bilateral ptosis (more pronounced on the right), hypertelorism, epicanthal folds, flat nasal bridge, anteverted nares, prominent deeply grooved philtrum, low-set and posteriorly angulated ears with thickened helices, short webbed neck with pterygium coli and low posterior hairline, pectus deformity, dark skin, multiple cutaneous nevi. Developmental milestones were in the normal range. The child sat at age 7 months, and walked alone at age 13 months. Language was mildly delayed and learning difficulties were identified. The subject underwent surgical intervention for bilateral palpebral ptosis at 4 years of age. He also underwent surgical repair of right cryptorchidism at age 10 years. Brain MRI, two-dimensional color-Doppler echocardiography, renal ultrasonography, audiometric evaluation, and electroencephalogram were all normal.

The subject is now 12 years old. His weight is 44 kg (75^{th}-90^{th} centile), height 145 cm (25^{th}-50^{th} centile), and OFC 51.5 cm (3^{rd}-10^{th} percentile). Psychometric evaluation using the Leiter scale documented an intelligence quotient (IQ) of 91. Learning difficulties, particularly in reading and mathematics, problems in the field of visual/perceptual abilities-organizational skills, and attention deficit were documented. Previously performed genetic tests include array CGH, as well as sequencing of the *PTPN11*, *SOS1*, *SOS2*, *RAF1*, *KRAS*, *BRAF*, *MEK1*, *MEK2*, *NRAS*, and *SHOC2* genes, which were all normal.

Subject 13-15 (Pat30153, Fat30153 and Aunt30153; Family 30153; p.Glu171Lys)

The proband is a female with a history of pectus deformity, pulmonary stenosis, ptosis requiring surgery, optic atrophy and broad neck with a webbed appearance. She had several dysmorphic facial features including a broad forehead, hypertelorism, bilateral ptosis, and upturned and broad nasal tip, long philtrum, and low-set ears. Her adult height was 144 cm ($<3^{rd}$ percentile). Her mother (who was identified to not carry the *CDC42* mutation) was also short (147 cm, $<3^{rd}$ percentile), suggesting a familial contribution to her short stature. Her mutation-positive father has a history of a pectus deformity as well as several similar dysmorphic facial features. His adult height was 167 cm. Her mutation-positive paternal aunt has short stature (154 cm) and pectus deformity. She is reported to have a similar built and facial gestalt as the other affected family members, but she has never been evaluated personally by one of the authors. She has myocardial insufficiency and cardiac rhythm disturbance requiring implantation of a pacemaker device. It is not clear whether her cardiac problems have resulted from a congenital heart abnormality. She was diagnosed with glaucoma leading to loss of vision on the right eye. A cataract was removed at the age of 58 years. The paternal uncle also has a history of a pectus deformity, his height is 165 cm, and shared some of the same dysmorphic facial features. He has a son who also has dysmorphic facial features. For both of them, DNA was not available for molecular analysis. Similar clinical features were observed in the molecularly confirmed affected aunt The grandfather is predicted to have the mutation, but this has not been molecularly confirmed. He has a history of a ptosis, pectus deformity as well, and his adult height was 155 cm. The family tree is shown in Figure S1.

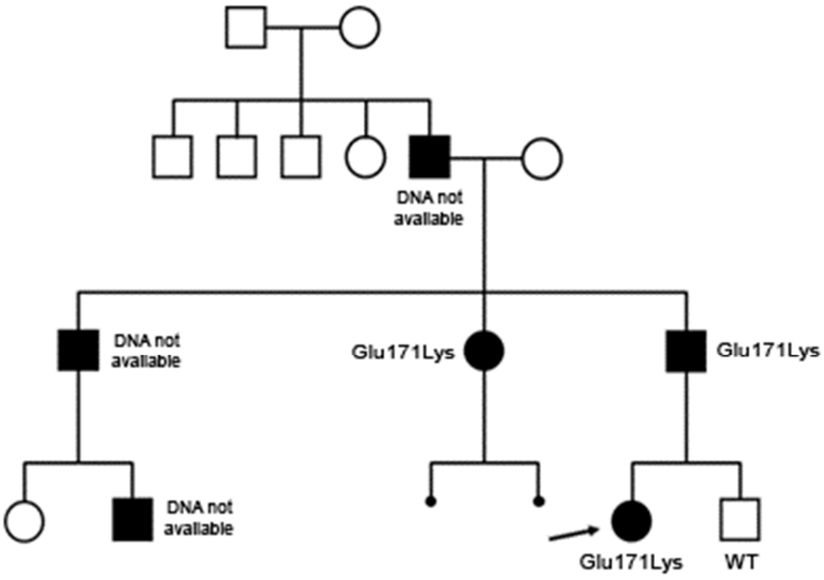

Figure S1. Pedigree of family 30153 showing transmission of the *CDC42* variant and its co-segregation with the trait. The affected index individual (subject 13) is indicated (arrow), together with the other genotypized members of the family, including her affected father and aunt (subjects 14 and 15), all of whom harbored the *CDC42* mutation (p.Glu171Lys). Three additional members of the family were clinically affected but DNA specimens were not available for mutation analysis.

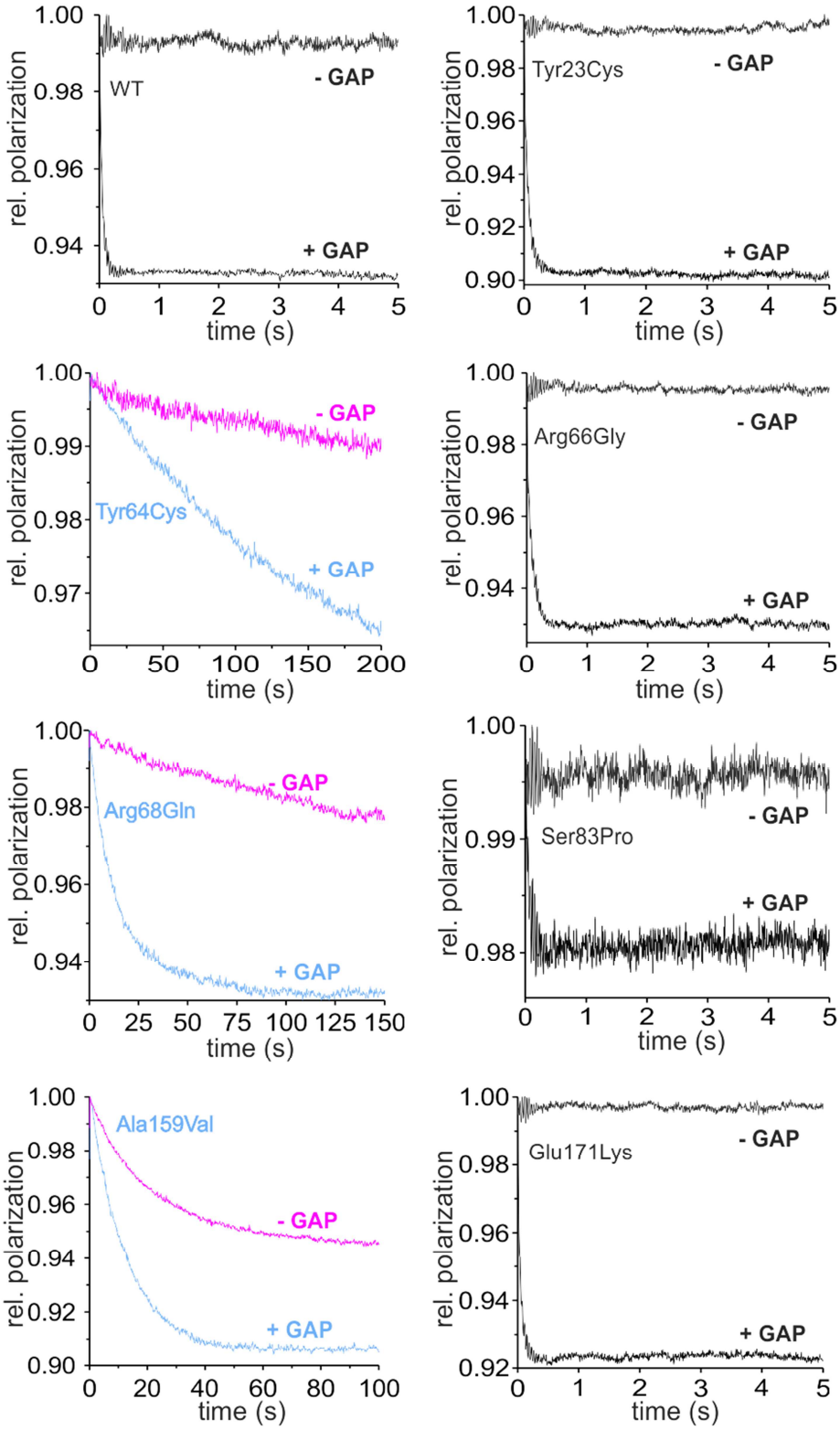

Figure S2. Basal and GAP-stimulated GTPase activity of disease-causing CDC42 mutants. Hydrolysis of tamraGTP was measured basally and following stimulation with ARHGAP1 ($p50^{GAP}$) in a stopped-flow machine. Although the $CDC42^{Tyr64Cys}$, $CDC42^{Arg68Gln}$ and $CDC42^{Ala159Val}$ mutants exhibited a slight ($CDC42^{Tyr64Cys}$, $CDC42^{Arg68Gln}$) or strong ($CDC42^{Ala159Val}$) increase in intrinsic GTP hydrolysis (magenta curves), they showed robust $p50^{GAP}$ insensitivity (blue curves). The data are represented as bar charts in **Figure 2A**.

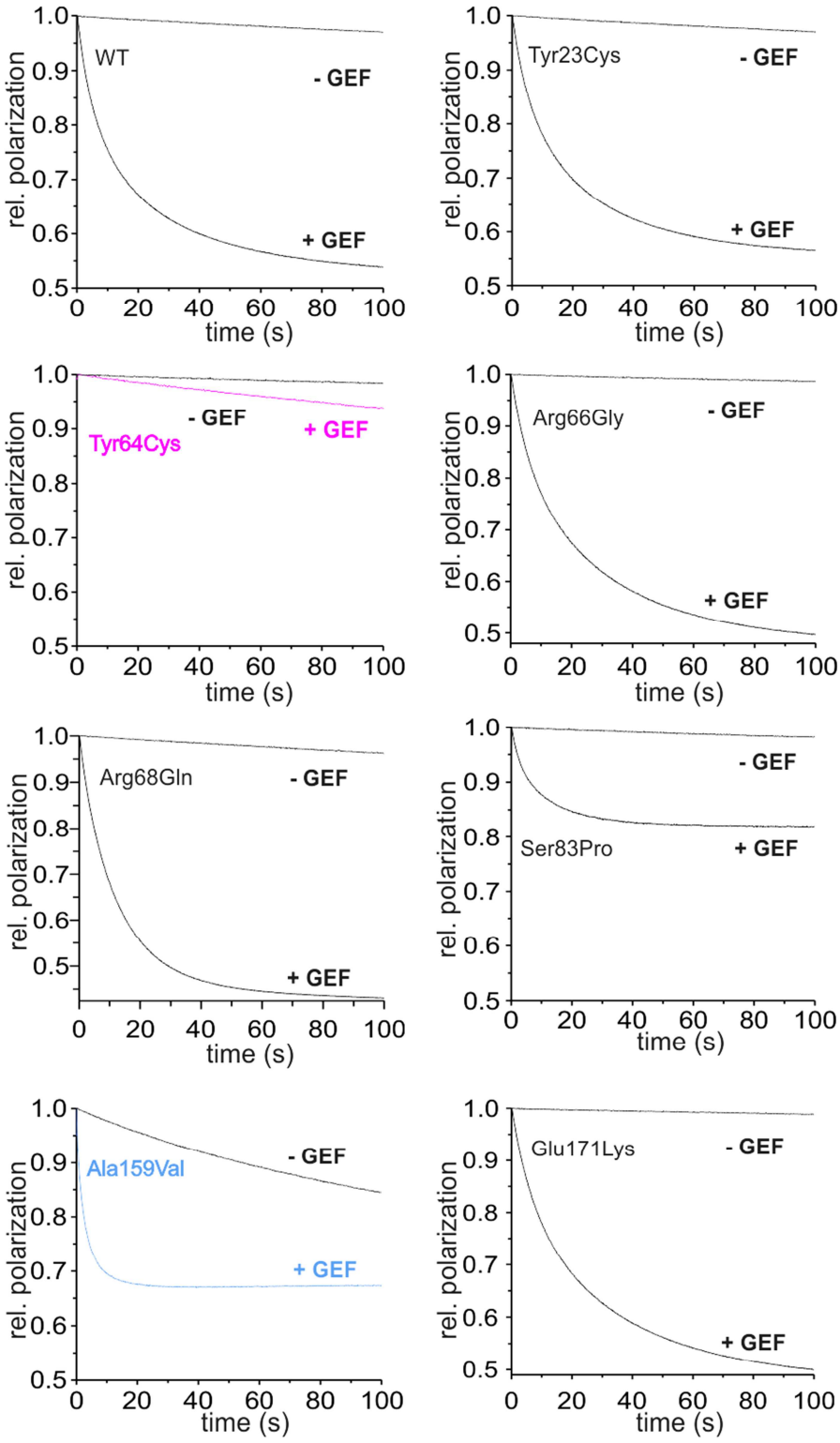

Figure S3. Basal and GEF-catalyzed nucleotide exchange reactions of disease-causing CDC42 mutants. The release of a fluorescently labelled GDP (mantGDP) was measured basally and with the catalytic domain of intersectin (ITSN1) in a stopped-flow machine. The CDC42^{Ala159Val} mutant exhibited a significantly increased intrinsic and GEF-catalyzed nucleotide release, while ITSN1 activity towards CDC42^{Tyr64Cys} was almost completely abolished (magenta curve). The data are represented as bar charts in **Figure 2B**.

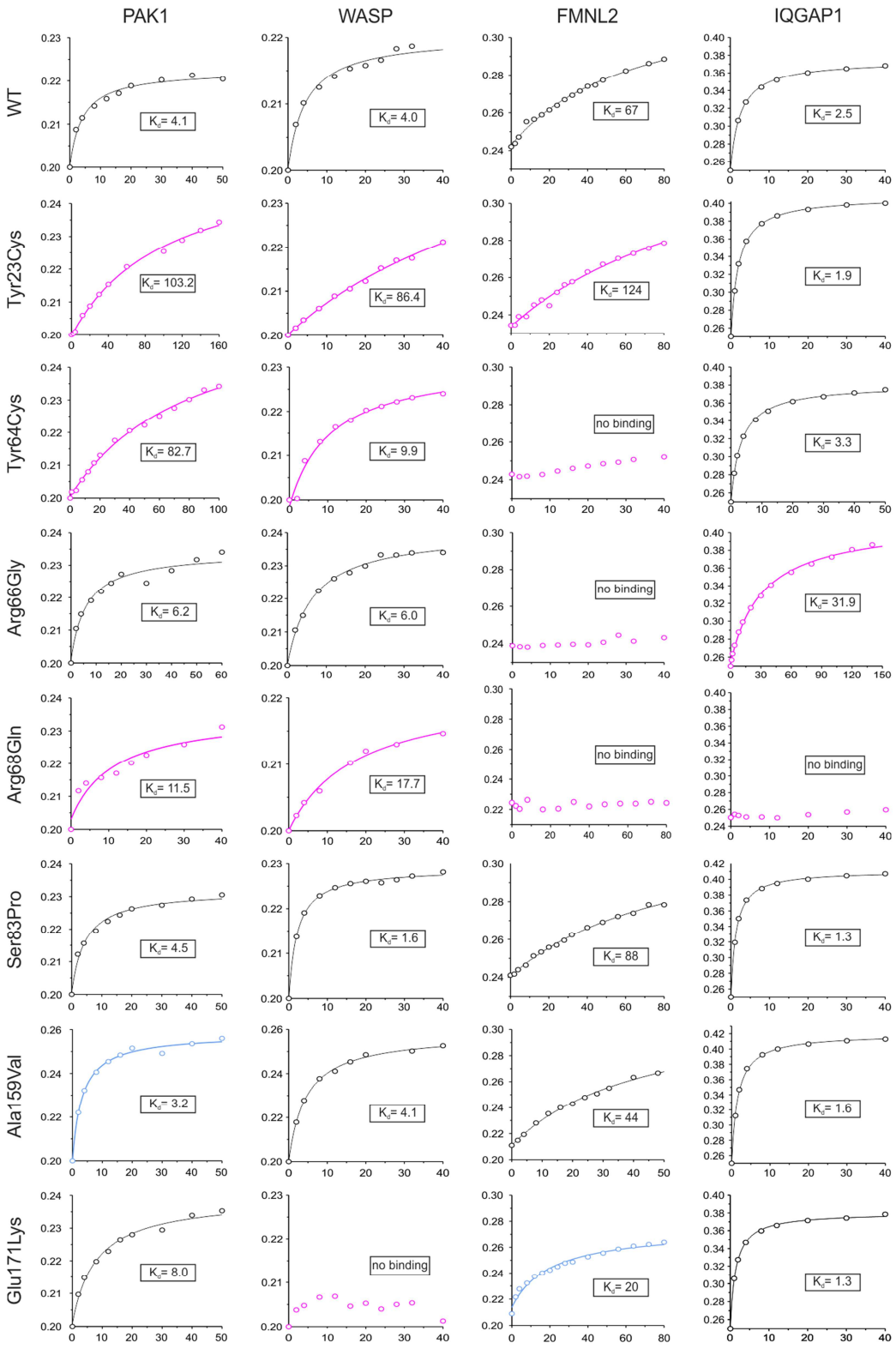

Figure S4. Binding of disease-causing CDC42 mutants to diverse effectors. Fluorescence polarization experiments were conducted to determine the dissociation constants (K_d) by titrating mantGppNHp-bound, active CDC42 variants with increasing concentrations of GTPase binding domains (GBD) of PAK1, WAS (WASP), FMNL2 and IQGAP1, as indicated. The y-axis represents fluorescence polarization, and the x-axis the concentration of the respective effector proteins as GST-fusion proteins in µM. Blue curves indicate increased binding affinity, whereas decrease or loss of binding is colored in magenta. Data are represented as bar charts in **Figure 2C**.

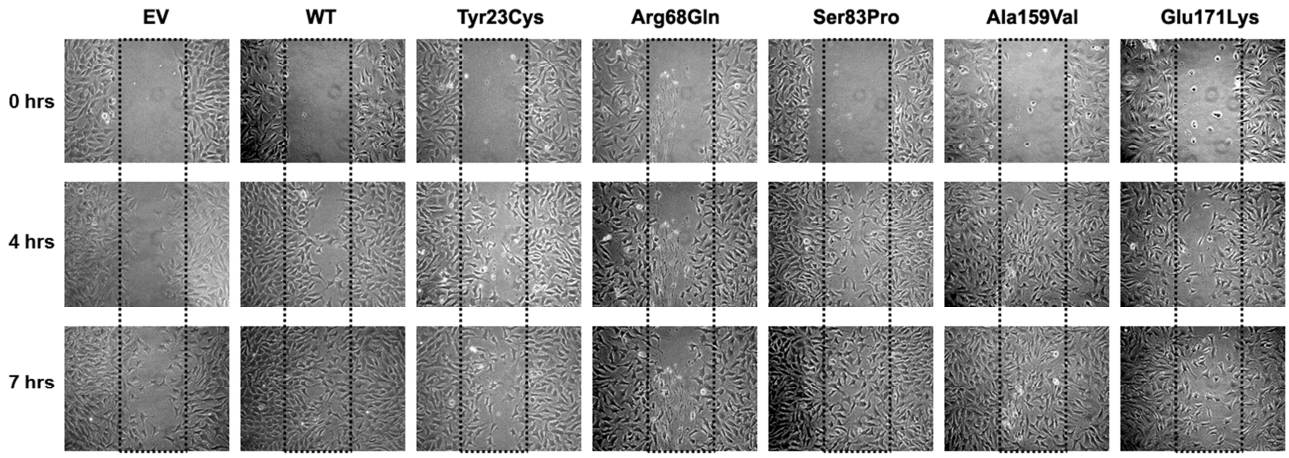

Figure S5. *CDC42* mutations differentially impact polarized migration. Wound-healing was performed using NIH3T3 cells transiently transfected to express wild-type CDC42 (WT), each of the $CDC42^{Tyr23Cys}$, $CDC42^{Arg68Gln}$, $CDC42^{Ser83Pro}$, $CDC42^{Ala159Val}$ and $CDC42^{Glu171Lys}$ mutants, or the relative empty vector (EV). A representative assay of three performed is shown. The wound was generated 24 hours after transfection, and migration in the wounded area was evaluated after, 0, 4 and 7 hours. Cells expressing exogenous wild-type CDC42 were shown to migrate more rapidly into the scratched area than cells transfected with the empty vector. Mutants were shown to differentially perturb polarized migration. Specifically, $CDC42^{Ser83Pro}$ and $CDC42^{Ala159Val}$ overexpression variably enhanced the wound closure ability of transfected cells compared to the wild-type protein, whereas expression of $CDC42^{Tyr23Cys}$, $CDC42^{Arg68Gln}$ and $CDC42^{Glu171Lys}$ failed to do that, supporting a gain-of-function and a loss-of-function effect of these mutants, respectively. Data are represented as bar charts in **Figure 3A**.

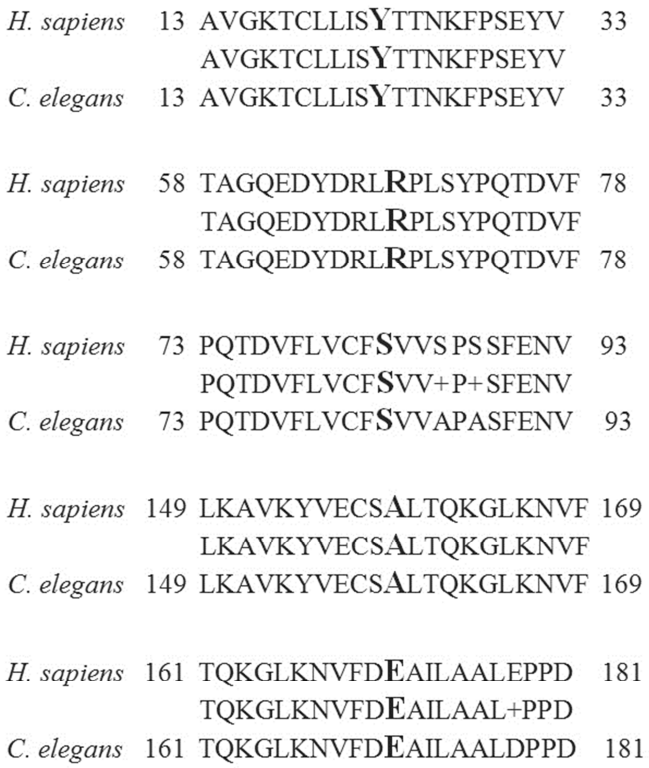

Figure S6. Amino acid sequence alignments of human CDC42 and the *C. elegans* ortholog. Stretches encompassing residues Tyr[23], Arg[68], Ser[83], Ala[159] and Glu[171] are shown, with affected residues shown in bold. Identity and conservation (+) of individual residues is also reported (middle row).

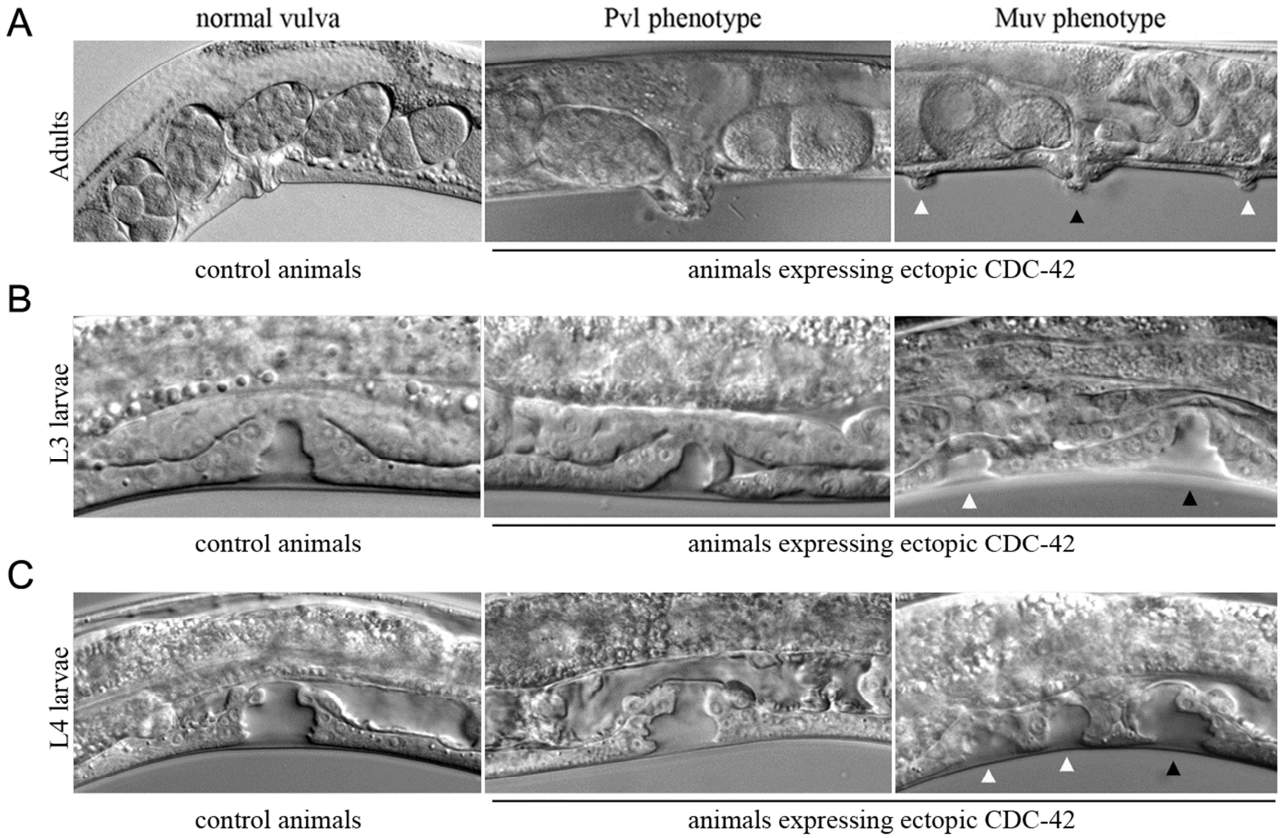

Figure S7. Consequences of *CDC-42* expression on vulval development in *C. elegans*. Ectopic expression of wild-type CDC-42 at the late L2/early L3 larval stages elicits multivulva (Muv) and protruding vulva (Pvl) phenotypes. Nomarski images show that a normal vulva develops in adult control animals (left), whereas a single protruding vulva (middle) or multiple ectopic pseudovulvae (right) are observed in a variable proportion of CDC-42-expressing animals (**A**). Black and white arrowheads point to the vulva and ectopic pseudovulvae, respectively. Nomarski images of vulval precursor cells (VPCs) at late L3 (**B**) and mid L4 (**C**) larval stages. In control animals, only P6.p descendants detach from the cuticle generating a single, symmetric invagination (left), whereas in CDC-42 expressing animals, VPCs descendants generates asymmetric invaginations (middle), or additional VPCs assume fate 1, generating multiple invaginations (right). Black and white arrowheads point to P6.p descendants-derived invagination and extra invaginations, respectively. Anterior is to the left and dorsal is up, in all images.

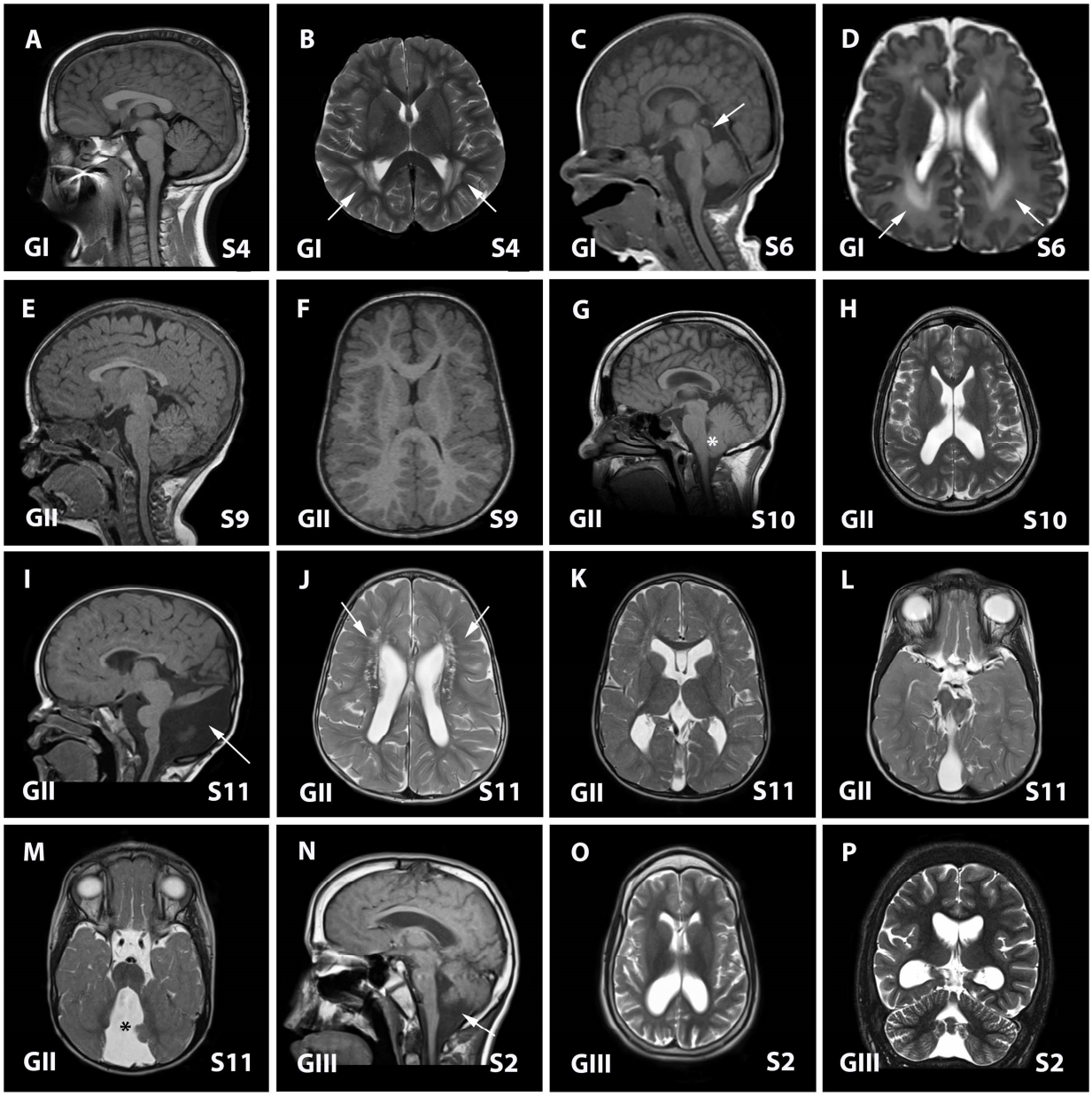

Figure S8. Brain MRIs of *CDC42* mutation-positive individuals. (**A-B**) Subject 4 (S4, p.Arg66Gly), T1-weighted mid-sagittal and T2-weighted axial images showing a thick corpus callosum, and white matter signal intensities in the posterior periventricular regions (arrows). (**C-D**) Subject 6 (S6, p.Arg68Gln), T1-weighted midsagittal and T2-weight axial images showing a thin corpus callosum, large tectum (arrow), mild ventriculomegaly, and white matter signal intensities in the posterior periventricular regions (arrows). (**E-F**) Subject 9 (S9, p.Ser83Pro), T1-weighted mid-sagittal and axial images showing a thin corpus callosum and deep cortical infolding (**G-H**) Subject 10 (S10, p.Ser83Pro), T1-weighted midsagittal and T2-weighted axial images showing mild cerebellar tonsillar ectopia (asterisk) and mild ventriculomegaly. (**I-M**) Subject 11 (S11, p.Ala159Val), T1-weighted para-sagittal and T2-weighted axial and coronal images showing a small and upward rotated cerebellar vermis consistent with a Dandy-Walker malformation (arrow, I; asterisk, M), thin corpus callosum, globular pons, white matter signal intensities in the frontal periventricular regions (arrows), mild ventriculomegaly, and asymmetric midbrain with a possible cleft in the tectum. (**N-P**) Subject 2 (S2, p.Tyr23Cys), T1-weighted para-sagittal and T2-weighted axial and coronal images showing a small and dysplastic cerebellar vermis (arrow, N), cerebral and cerebellar atrophy, and ventriculomegaly. Mutation groups (GI to GIII) are indicated.

Table S1. WES data output of *CDC42* mutation-positive individuals.

ID	WES enrichment kit	Sequencing platform	Target regions covered >10x	Target regions covered >20x	Average depth on target
Subject 1 (LR16-483)	SureSelect Clinical Research Exome	Illumina HiSeq2000	98.2%	96.4%	159x
Subject 2 (LR14-224)	SureSelect Human All Exon v1	Illumina HiSeq2000	91.2%	86.6%	110x
Subject 3 (LR17-420)	Nextera Exome Enrichment Kit	Illumina HiSeq2000	99.5%	99.0%	188x
Subject 4 (LR14-352)	SeqCap EZ VCRome 2.0	Illumina HiSeq2000	97.1%	94.3%	121x
Subject 5 (PCGC 1-04248)	SureSelect Human All Exon v5	Illumina HiSeq2000	98.3%	85.2%	82x
Subject 8 (LR17-032)	SureSelect Clinical Research Exome	Illumina HiSeq2000	97.0%	94.5%	104x
Subject 9 (LR10-046)	SeqCap EZ MedExome v2	Illumina HiSeq2000	89%	79%	57.2x
Subject 10 (LR16-056)	SureSelect Human All Exon v3	Illumina HiSeq2000	97.1%	85.3%	83.8x
Subject 11 (LR15-338)	SeqCap EZ MedExome v2	Illumina HiSeq2000	90%	80%	110x

Table S2. Interpretation of the identified *CDC42* variants according to ACMG criteria.

Amino acid change	Combining criteria for pathogenicity	ACMG codes	Specific criteria	ACMG classification
p.Ile21Thr	1 Strong, 2 Moderate and ≥2 Supporting	PS2; PM1, PM2; PP2, PP3	*de novo*; affecting a functional domain, absent in public databases; missense variant, variant predicted to be pathogenic	Pathogenic
p.Tyr23Cys	≥2 Strong	PS2, PS3	*de novo*; *in vitro*/*in vivo* functional studies documenting impact on protein function	Pathogenic
p.Tyr64Cys	≥2 Strong	PS1, PS2, PS3	known pathogenic variant; *de novo*; *in vitro* functional studies documenting impact on protein function	Pathogenic
p.Arg66Gly	≥2 Strong	PS2, PS3	*de novo*; *in vitro* functional studies documenting impact on protein function	Pathogenic
p.Arg68Gln	≥2 Strong	PS2, PS3	*de novo*; *in vitro*/*in vivo* functional studies documenting impact on protein function	Pathogenic
p.Cys81Phe	1 Strong, 2 Moderate and ≥2 Supporting	PS2; PM1, PM2; PP2, PP3	*de novo*; affecting a functional domain; absent in public databases; missense variant; predicted to be pathogenic	Pathogenic
p.Ser83Pro	≥2 Strong	PS2, PS3	*de novo*; *in vitro*/*in vivo* functional studies documenting impact on protein function	Pathogenic
p.Ala159Val	≥2 Strong	PS2, PS3	*de novo*; *in vitro*/*in vivo* functional studies documenting impact on protein function	Pathogenic
p.Glu171Lys	≥2 Strong	PS2, PS3	*de novo*; *in vitro*/*in vivo* functional studies documenting impact on protein function	Pathogenic

PS, pathogenic strong; PM, pathogenic moderate; PP, pathogenic supporting.
PS1: same amino acid change as a previously established pathogenic variant regardless of nucleotide change.
PS2: *de novo* (both maternity and paternity confirmed) in an affected subject with the disease and no family history.
PS3: well-established *in vitro* or *in vivo* functional studies supportive of a damaging effect on the gene or gene product.
PM1: located in a mutational hot spot and/or critical and well-established functional domain without benign variation.
PM2: absent from controls (or at extremely low frequency if recessive) in Exome Sequencing Project, 1000 Genomes or ExAC.
PP2: missense variant in a gene that has a low rate of benign missense variation and where missense variants are a common mechanism of disease.
PP3: multiple lines of computational evidence support a deleterious effect on the gene or gene product (e.g., conservation, evolutionary, splicing impact).

Table S3. Vulval phenotypes in nematodes expressing wild-type CDC-42 or the disease-associated mutants.

Genotype	Transgene	Pvl (%)	Muv (%)	Vul (%)	N
wild-type	-	0.5	0	0	>2000
wild-type	empty vector	0.9	0	0	233
wild-type	*cdc-42*^{WT}	18.3[a]	2.3[d]	0	1447
wild-type	*cdc-42*^{Tyr23Cys}	8.1[a,b]	2.9[d]	0	588
wild-type	*cdc-42*^{Arg68Gln}	12.6[a,c]	2.0[d]	0	810
wild-type	*cdc-42*^{Ser83Pro}	31.0[a,b]	4.5[d,c]	0	749
wild-type	*cdc-42*^{Ala159Val}	34.3[a,b]	5.8[d,e]	0	572
wild-type	*cdc-42*^{Glu171Lys}	8.5[a,b]	2.1[d]	0	943
let-60(n1046)	-	na	72.5	0	501
let-60(n1046)	*cdc-42*^{WT}	na	89.2[f]	0	182
let-23(sy1)	-	0	0	80.2	956
let-23(sy1)	*cdc-42*^{WT}	0	0	47.4[g]	475
let-23(sy1)	*cdc-42*^{Tyr23Cys}	0	0	47.5[g]	133
let-23(sy1)	*cdc-42*^{Arg68Gln}	0	0	47.8[g]	251
let-23(sy1)	*cdc-42*^{Ser83Pro}	0	0	30.2[g,h]	374
let-23(sy1)	*cdc-42*^{Ala159Val}	0	0	21.6[g,h]	236
let-23(sy1)	*cdc-42*^{Glu171Lys}	0	0	49.4[g]	166

Strains: *let-60(n1046)* is a gain-of-function allele of *let-60/RAS*; *let-23(sy1)* is a hypomorphic allele of *let-23/EGFR*.

Wild-type and mutant *cdc-42* alleles were expressed under the control of the *hsp16.41* inducible promoter. Animals were grown at 20 °C and heat-shocked at late L2/early L3 stages. *N* indicates the number of animals scored. Multivulva (Muv), protruding vulva (Pvl) and vulvaless (Vul) phenotypes are expressed as percentage of adults with ectopic pseudovulvae, exhibiting a protruding vulva or lacking a vulva, respectively.

na: not ascertained.

In all comparisons, *P*-values were calculated using two-tailed Fisher's exact test.

[a]Significantly different from animals expressing the empty vector ($P < 0.00005$).

[b]Significantly different from animals expressing *cdc-42*^{WT} ($P < 0.0001$).

[c]Significantly different from animals expressing *cdc-42*^{WT} ($P < 0.05$).

[d]Significantly different from animals expressing the empty vector ($P < 0.05$).

[e]Significantly different from animals expressing *cdc-42*^{WT} ($P < 0.001$).

[f]Significantly different from *let-60(n1046)* animals ($P < 0.00001$).

[g]Significantly different from *let-23(sy1)* animals ($P < 10^{-12}$).

[h]Significantly different from *let-23(sy1)* animals expressing *cdc-42*^{WT} ($P < 0.0001$).

Table S4. Impact of *wsp-1*/*WASP* RNA-mediated interference on vulval phenotypes in *C. elegans*.

Genotype	Transgene	Gene Modulated by RNAi	Time of exposure to RNAi bacteria (hours)	Pvl (%)	Muv (%)	N
let-60(n1046)	-	*let-60*	0	na	73.2	205
			2	na	44.0[a]	150
			4	na	34.2[a]	117
			8	na	25.8[a]	120
wild-type	-	*wsp-1*	0	0.7	0	150
			8	1.3	0.2	829
wild-type	*cdc-42^{WT}*	*wsp-1*	0	21.4	2.4	627
			2	19.5	1.8	56
			4	13.5[b]	1.8	168
			8	11.7[c]	4.1	410
wild-type	*cdc-42^{Tyr23Cys}*	*wsp-1*	0	7.5	2.6	154
			2	8.0	2.5	122
			4	7.1	2.4	85
			8	6.8	2.8	72
wild-type	*cdc-42^{Arg68Gln}*	*wsp-1*	0	13.6	2.7	86
			2	14.1	2.0	105
			4	12.5	2.8	72
			8	9.8	3.2	96
wild-type	*cdc-42^{Ser83Pro}*	*wsp-1*	0	31.2	4.2	214
			2	30.0	3.8	78
			4	35.0	4.0	101
			8	42.0[b]	4.9	205
wild-type	*cdc-42^{Ala159Val}*	*wsp-1*	0	42.3	6.3	189
			2	45.0	6.3	79
			4	48.0	5.9	119
			8	49.3	7.7	143
wild-type	*cdc-42^{Glu171Lys}*	*wsp-1*	0	8.7	2.3	263
			2	8.8	1.9	54
			4	8.3	2.2	89
			8	9.4	1.6	124

Synchronized adult hermaphrodites were left on agar plates seeded with RNAi bacteria for the indicated time. Screening of the protruding vulva (Pvl) and multivulva (Muv) phenotypes was carried out on F1 animals grown at 20 °C and heat-shocked at early L3 larval stage. *N* indicates the number of animals scored. As a control of the efficiency of the RNAi protocol, *let-60* RNAi was performed on animals carrying the activating p.Gly13Glu substitution in LET-60, which is associated with a high penetrant Muv phenotype.

wsp-1 RNAi had no vulva phenotype *per se*, but was shown to significantly reduce the prevalence of Pvl associated with expression of CDC-42^{WT} ($P < 0.0001$), indicating that occurrence of this phenotype is mediated, in part, by WSP-1. In contrast, the vulval defect observed in CDC-42^{Tyr23Cys}, CDC-42^{Arg68Gln} and CDC-42^{Glu171Lys} animals was not modulated by *wsp-1* RNAi, which is consistent with the collected biochemical data indicating abolished (CDC-42^{Glu171Lys}) or strongly reduced (CDC-42^{Tyr23Cys} and CDC-42^{Arg68Gln}) association of these mutants with WASP. The Muv phenotype was not modulated by *wsp-1* RNAi. *P*-values were calculated using two-tailed Fisher's exact test; na, not ascertained.

[a]Significantly different from non-interfered *let-60(n1046)* animals ($P < 0.0001$).

[b]Significantly different from the corresponding non-interfered animals ($P < 0.05$).

[c]Significantly different from the corresponding non-interfered animals ($P < 0.0001$).

Table S5. Clinical features of *CDC42* mutation-positive individuals.

Subject	1	2	3	4	5	6	7	8	9	10	11	12	13	14	15
ID	**LR16-483**	**LR14-224**	**LR17-420**	**LR14-352**	**PCGC 1-04248**	**ISS3MO**	**ISS4BO**	**LR17-032**	**LR10-046**	**LR16-056**	**LR15-338**	**M060721**	**Pat30153**	**Fat30153**	**Aunt30153**
Mutation group	**III**	**III**	**I**	**I**	**I**	**I**	**I**	**II**	**II**	**II**	**II**	**III**	**III**	**III**	**III**
Mutation	**p.I21T**	**p.Y23C**	**p.Y64C**	**p.R66G**	**p.R66G**	**p.R68Q**	**p.R68Q**	**p.C81F**	**p.S83P**	**p.S83P**	**p.A159V**	**p.E171K**	**p.E171K**	**p.E171K**	**p.E171K**
Sex	M	M	F	M	F	M	F	M	M	M	M	M	F	M	F
Age last assessed	10y	14y	15y	18y	8m	4y	5y	4y	6y	34y	6y	12y	Adult	Adult	Adult
Growth															
Birth weight	–2 SD	–1.5 SD	-2 SD	–4 SD	ND	0 SD	0 SD	–1.5 SD	0 SD	–0.75 SD	–2 SD	–1 SD	+0.25 SD	ND	ND
Birth OFC	ND	–2 SD	–2.2 SD	ND	ND	–0.25 SD	+1.5 SD	ND	ND	0 SD	–3 SD	–1 SD	ND	ND	ND
Postnatal weight	ND	–1 SD	–0.9 SD	–5 SD	–5 SD	–2.4 SD	–1.3 SD	ND	–1.5 SD	+2 SD	–2 SD	+0.5 SD	–2.5 SD	–1.5 SD	ND
Postnatal OFC	–2 SD	–3.5 SD	–4.3 SD	–0.5 SD	–3.5 SD	–2 SD	+0.25 SD	–2.6	+2 SD	0 SD	–3 SD	–1.7 SD	–3.5 SD	ND	ND
Postnatal growth deficiency	+	+	+	+	+	+	–	+	+	+	+	–	+	–	+
Neurologic Abnormalities															
DD/ID	+, no IQ testing, ADHD	++	++	++	+	++	++	++	++	++	++	–	–	–	–
Seizures	–	+	–	–	ND	–	+, 4 febrile	–	+	+, myoclonic	–	–	–	–	–
Tone	H	H	H, C	H	ND	C	–	–	–	C	H/C	–	–	–	–
Endocrine Issues															
Low GH	ND	+	–	+	ND	–	–	–	+	–	–	–	–	–	–
Hypothyroidism	ND	–	+	–	ND	–	–	–	+	–	–	–	–	–	–
Immunodeficiency	ND	–	+	+	ND	–	–	–	–	–	–	–	–	–	–
Other system abnormalities															
Hands-feet	ND	CD	CD, distal arthrogryposis	S	–	–	Long thin fingers	–	–	S/CD	S/CD	–	–	–	–
Eye abnormalities	Myopia	OA	Pale ON	Hyperopia, ST, OA, thick corneas	ND	ST	Astigmatism	ST	ST	ST	ST, OMP	Myopia, ST	ST, OA	–	GL, CA

Table S5 (continued)

Subject	1	2	3	4	5	6	7	8	9	10	11	12	13	14	15
ID	**LR16-483**	**LR14-224**	**LR17-420**	**LR14-352**	**PCGC 1-04248**	**ISS3MO**	**ISS4BO**	**LR17-032**	**LR10-046**	**LR16-056**	**LR15-338**	**M060721**	**Pat30153**	**Fat30153**	**Aunt30153**
Mutation group	**III**	**III**	**I**	**I**	**I**	**I**	**I**	**II**	**II**	**II**	**II**	**III**	**III**	**III**	**III**
Mutation	**p.I21T**	**p.Y23C**	**p.Y64C**	**p.R66G**	**p.R66G**	**p.R68Q**	**p.R68Q**	**p.C81F**	**p.S83P**	**p.S83P**	**p.A159V**	**p.E171K**	**p.E171K**	**p.E171K**	**p.E171K**
Skin	Several CALs	–	exzema	Multiple nevi	–	Maculopapular cutaneous eruption	–	–	–	–	–	Multiple nevi	–	–	–
Pectus	ND	–	–	–	–	+	–	–	–	–	–	+	+	+	+
Scoliosis	+	+	+	+	–	–	–	–	+	–	–	–	–	–	–
Inguinal hernia	+	+	+	–	–	+	+, bilateral	–	–	+	–	–	–	–	–
Cardiac defects	ND	–	ASD/VSD/PDA	–	–	HCM	VSD/PFO	–	TAPVR coarctation	–	PFO	–	Pulmonary stenosis	–	MI
GU defects	Unilateral renal agenesis	–	Renal pelviectasis	Renal dysplasia	–	–	–	Penile webbing	–	–	Hypospadias	–	–	–	–
Lymphatic malformations	–	–	–	+ pericardial effusion	–	–	–	–	–	+ pericardial effusions/gut	–	–	–	–	–
Platelets Large/Low	ND	–/–	+/+	+/–	ND	–/+	+/+	–	–/–	+/–	ND	–	–	–	ND
Recurrent Infections	+, recurrent OM	–	+	+	–	+	+	+	+	+	–	–	–	–	–

Abbreviations: ADHD, attention-deficit hyperactivity disorder; CALs, café au lait spots; C, contractures; CA, cataract; CD, camptodactyly; DD, developmental delay; F, female; GL, glaucoma; H, hypotonia; HCM, hypertrophic cardiomyopathy; ID, intellectual disability; m, month; M, male; MI, myocardial insufficiency; MPV, mean platelet volume; ND, no data; OA optic atrophy; OFC, occipitofrontal circumference; OM, otitis media; OMP, oculomotor palsy; ON, optic nerves; PFO, patent foramen ovale; S, syndactyly; SD, standard deviations; ST, strabismus; TAPVR, total anomalous pulmonary venous return; VSD, ventricular septal defect; y, year.

Table S6. Details of the facial features of *CDC42* mutation-positive individuals.

Subject	1	2	3	4	5	6	7	8	9	10	11	12	13	14
ID	**LR16-483**	**LR14-224**	**LR17-420**	**LR14-352**	**PCGC 1-04248**	**ISS3MO**	**ISS4BO**	**LR17-032**	**LR10-046**	**LR16-056**	**LR15-338**	**M060721**	**Pat30153**	**Fat30153**
Mutation group	**III**	**III**	**I**	**I**	**I**	**I**	**I**	**II**	**II**	**II**	**II**	**III**	**III**	**III**
Mutation	**p.I21T**	**p.Y23C**	**p.Y64C**	**p.R66G**	**p.R66G**	**p.R68Q**	**p.R68Q**	**p.C81F**	**p.S83P**	**p.S83P**	**p.A159V**	**p.E171K**	**p.E171K**	**p.E171K**
Sex	M	M	F	M	F	M	F	M	M	M	M	M	F	M
Age last assessed	10y	14y	15y	16y	8m	4y	5y	4y	6y	34y	6y	12y	Adult	Adult
Hair	ND	–	W	W	–	S/W	S	–	W	S/W	S	S	ND	ND
Eyebrows	ND	–	MF	–	–	S	S	–	–	–	S	S	–	–
Forehead	P	–	Short	B	–	P	B/P	B/P	B/P	P	P	–	B	B
Hypertelorism	ND	–	+	–	–	+	+ (mild)	+	+	+	+	+	+	–
Wide PF	+	+	–	–	–	–	–	+	–	–	+	+	–	–
Everted LE	ND	–	–	–	–	–	–	–	–	–	–	+	–	ND
Epicanthal folds	ND	+	–	–	–	+	–	+	–	–	–	+	+	–
Ptosis	–	+, U	–	+, B	–	–	–	+, B	–	+, B	+, B	+, B	+, B	–
Nasal bridge	H/N	H	N	H/N	–	W	W	W	W	W	W	W	W	–
Flared nostrils	–	–	+	–	–	+	+	+	–	+	–	+	+	–
Nasal tip Up/Broad	Broad	Up	Broad	Broad	–	Broad	Broad	Broad	–	–	Broad	Broad	Up/ broad	Up/ broad
Low-hanging columella	–	+	++	–	–	–	–	–	–	–	–	–	–	–
Underdeveloped midface	+	–	+	–	–	+	+	+	–	–	+	–	–	–
Philtrum	–	Short	Short	–	–	Long	Long	Long	Long	–	–	Deep	Long	Long
Thin upper vermillion	–	–	++	+	–	+	+	+	+	–	–	+	+	+
Mouth	CD/W	CD	W	W	–	–	CB	+	CB/W	W	CB/W	–	CD	–
Ears	L	–	S, LS	–	–	TH	LS	LS	LS	–	–	L/LS	LS	LS
Other facial features	Synophrys, PMS	Long neck	UPF, MF, small chin	Cleft palate, WSP	–	Neck webbing	–	–	Broad jaw, WSP	Broad jaw, WSP	–	Neck webbing	Neck webbing	Neck webbing

Abbreviations (ordered by feature): Hair: sparse (S), whorls (W); Eyebrows: medial flared (MF), sparse (S); Forehead: broad (B), prominent (P); PF, palpebral fissures; LE, lateral eyelids; Ptosis: unilateral (U), bilateral (B); Nasal bridge: high (H), narrow (N), wide (W); Mouth: cupid bow (CB), corners down (CD), wide (W); Ears: large (L), low-set (LS), small (S), thick helix (TH); UPF, upslanting palpebral fissures; PMS, prominent metopic suture; WPS, widely spaced teeth.

Table S7. Neuroimaging features of *CDC42* mutation-positive individuals.

Subject	**1**	**2**	**3**	**4**	**6**	**7**	**8**	**9**	**10**	**11**
ID	**LR16-483**	**LR14-224**	**LR17-420**	**LR14-352**	**ISS3MO**	**ISS4BO**	**LR17-032**	**LR10-046**	**LR16-056**	**LR15-338**
Mutation group	**III**	**III**	**I**	**I**	**I**	**I**	**II**	**II**	**II**	**II**
Mutation	**p.I21T**	**p.Y23C**	**p.Y64C**	**p.R66G**	**p.R68Q**	**p.R68Q**	**p.C81F**	**p.S83P**	**p.S83P**	**p.A159V**
Age at scan	13m	12y	3y	ND	5m	ND	34y	3y	34y	3y
Cortex	–	Diffuse atrophy	–	–	–	SEH	–	–	–	–
White matter	–	Decreased	Mildly thin	Mildly prominent PV WM signal intensities (posteriorly)	Mildly prominent PV WM signal intensities (posteriorly)	-	–	Mild periventricular WM abnormalities (PVL)	–	WM signal intensities
Ventricles, extra-axial space	–	VMEG	VMEG	–	VMEG, increased extra-axial space	–	–	Hydrocephalus s/p shunting	VMEG	–
Corpus callosum	–	Thin	Thin	Mildly thick	Mildly thin	pACC	Mild pACC	Mildly thin	–	pACC
Cerebellum	–	Diffuse atrophy, mild vermis hypoplasia	–	–	–	–	Mega cisterna magna	–	CBTE	Large PF, cerebellar foliar dysplasia, large ICP, small MCP, stretched SCP, severe DWM
Basal ganglia/thalami	–	–	–	–	–	–	–	–	–	Dysplastic thalami
Brainstem	–	–	–	–	Large tectum	–	–	–	–	Small medulla/pons, cleft in the tectum, abnormal superior colliculi
Hippocampi	–	–	–	–	–	–	–	–	–	Unilateral HIP dysplasia

Abbreviations: pACC, partial agenesis of the corpus callosum; CBTE, cerebellar tonsillar ectopia; DWM, Dandy-Walker malformation; HIP, hippocampal dysplasia; ICP, inferior cerebellar peduncle; MCP, middle cerebellar peduncle; PF, posterior fossa; PV, perivascular; PVL, periventricular leukomalacia; SCP, superior cerebellar peduncle; SCV, small cerebellar vermis; SEH, subependymal heterotopia; VMEG, ventriculomegaly; WM, white matter.